

Master's Thesis

Calculations on radiation effects on electronics for ESS

Johannes C. Kazantzidis



Mapping, Analysis and Protection of Electronic
Circuits Against Radiation in the Accelerator
Tunnel of the ESS

Author:

Johannes C. Kazantzidis
ae110jka@student.lu.se

Company:

European Spallation Source, ESS

Advisors:

Riccardo Bevilacqua, ESS
Anders J. Johansson, LTH
Hanna Holstein, LU

February 14, 2015

Printed in Sweden
E-huset, Lund, 2015

Abstract

Estimation of radiation damage to electronics is complex and requires knowledge of several disciplines. Such estimation is important in the assessment of design and construction of systems in radiatory applications. This can be used to approximate the lifetime of electronics and to develop strategies for both ensuring reliability of the equipment and for financial optimization. To understand the interaction of radiation with matter, nuclear physics and the concept of fundamental forces and cross sections has been applied. Physics of devices has been investigated in order to understand the different types of damage and errors that may occur as a consequence of irradiation. Lastly, mapping and analysis of radiation, as well as response functions of electronics, are needed to predict radiation damage. Monte Carlo N-Particle Transport Code (MCNP) has been used to calculate the gamma and neutron radiation in the front-end building of the European Spallation Source. The radiation has been characterized in terms of quantities and energy spectra. STRAM is a software tool developed in this project, for revealing the radiation absorbed by electronics. The tool folds radiation maps with response functions of electronics, thus determining the absorbed dose. Consequently, this can be used to find the optimal location of a device, should it be feasible to be chosen arbitrarily. Otherwise, necessary shielding measures or conclusions regarding other options, can be derived from the results. This report presents research regarding radiation effects on electronics as well as the capabilities of STRAM for estimation of radiation damage. STRAM demonstrates applicability in all radiatory environments, provided a radiation map is generated.

Acknowledgements

I would like to express my gratitude to Riccardo Bevilacqua for his teaching, support and guidance throughout this project. I thank Konstantin Batkov for educational conversations and programming aid. I thank Luisella Lari for her inputs and former research. I also thank Anders J. Johansson and Hanna Holstein for following up on my work and including me in radiation experiments and educational visits to several research facilities. Furthermore, I thank Erik Lind for stimulating discussions regarding physics of devices. I also thank Günter Muhrer, Michał Jarosz, Benjamin Cheymol, Aurélien Ponton, Nick Gazis, Fernando Sordo, Eduardo Nebot Del Busto and Yukinobu Watanabe for contributing to the research. I also thank Dmitri Ivanov for reviewing and commenting on this report. I thank my beloved, Sabina Linderöth, for reviewing the report and for general support. Finally, I thank friends and family for supporting me during my studies.

Table of Contents

Abstract	i
Acknowledgements	iii
List of Figures	viii
List of Tables	ix
List of Abbreviations	xi
1 Introduction	1
1.1 Motivation	1
1.2 Project specification	1
1.3 Contributions	3
1.4 Thesis outline	3
2 Background	5
2.1 Nuclear physics	5
2.1.1 Elementary particles and fundamental forces	5
2.1.2 Nuclear reactions	7
2.1.3 Cross section	8
2.2 Electronics and physics of devices	9
2.2.1 p-n junction	9
2.2.2 Diode	10
2.2.3 Photodiode	12
2.2.4 Bipolar junction transistor	13
2.2.5 MOSFET	15
3 ESS	19
3.1 Spallation	19
3.2 Linear accelerator	20
3.2.1 Front-End Building	20
3.2.2 Accelerator tunnel	22
3.2.3 Target station	22

4	Radiation	25
4.1	Radiation effects on human tissue	25
4.2	Radiation weighting factors	26
4.3	Radiation effects on electronics	28
4.3.1	Cumulative Effects	29
4.3.2	Single Event Effects	30
4.3.3	Neutron induced soft errors	31
4.3.4	Limitations	34
4.3.5	Radiation hardness calibration	35
5	Simulations	37
5.1	Central Limit Theorem	37
5.2	Monte Carlo Methods	37
5.3	Monte Carlo radiation transport codes	38
5.3.1	FLUKA	38
5.3.2	Monte Carlo N-Particle Transport Codes	38
6	Software Development	39
6.1	ROOT	39
6.2	STRAM	40
6.2.1	Radiation map	40
6.2.2	Response function	42
6.2.3	Absorption map	42
6.2.4	GUI	43
7	Evaluation and conclusion	45
7.1	Radiation effects on electronics	45
7.2	STRAM	46
7.3	Improvements and future work	46
7.3.1	Radiation weighting factors for electronics	46
7.3.2	Chebyshev nodes	47
7.3.3	Location optimization in STRAM	47
7.3.4	Shielding investigation in STRAM	48
7.3.5	Web based version of STRAM	48
	Bibliography	49
	Appendix A Software Documentation	53
	Appendix B Chebyshev Interpolation Example	59
	Appendix C CERN Data	61
	Appendix D Radiation Effects on Cameras	65
	Appendix E L.E.N.A Experiment Guideline Proposal	67

List of Figures

2.1	The standard model of elementary particles	6
2.2	Arrow and apple cross section analogy.	9
2.3	p-n junction	10
2.4	Diffusion current	11
2.5	Space charge region with applied voltage	12
2.6	Effect of absorption on the quantum efficiency	13
2.7	BJT regions and biasing	14
2.8	Electrons in a BJT	14
2.9	BJT signal amplification	15
2.10	MOSFET inversion channel	16
2.11	I_{DS} as a function of U_{DS} in a MOSFET	17
3.1	ESS Linac	20
3.2	Preliminary schematics of the FEB	21
4.1	Radiation weighting factors for neutrons.	28
4.2	Charge build-up and removal in a MOSFET	30
4.3	Soft error contribution of incident-neutron energy range in NMOSFET	32
4.4	Soft error contribution of incident-neutron energy range in NMOSFET	33
4.5	SERs per bit	34
6.1	Chart of idea for absorption map	40
6.2	Radiation map example	41
6.3	Hypothetic radiation in the FEB	41
6.4	Nitrogen response function for γ -radiation	43
6.5	STRAM initial interface.	44
6.6	STRAM interface during interaction.	44
B.1	Chebyshev interpolation	60
C.1	Nitrogen response function for neutrons	62
C.2	Nitrogen response function and neutron cross section	63
C.3	Nitrogen response function for gammas	63
C.4	Recomputed response function and absorption map.	64

D.1	Dead camera pixels due to radiation	65
-----	---	----

List of Tables

2.1	Fundamental forces and Boson mediators.	5
2.2	Fundamental interactions.	6
2.3	Properties of quarks and antiquarks	7
4.1	Radiation weighting factors from SSM's regulatory rode	26
4.2	Radiation weighting factors from SSM's special conditions for the ESS	27
4.3	Radiation weighting factors from ICRP Publication 60	28
4.4	Fraction of incident neutron flux	33

List of Abbreviations

BJT	Bipolar Junction Transistor
DTL	Drift Tube Linac
ESS	European Spallation Source
FEB	Front-End Building
FLUKA	Fluktuierende Kaskade
LHC	Large Hadron Collider
LEBT	Low Energy Beam Transport
Linac	Linear accelerator
MCNP	Monte Carlo N-Particle
MEBT	Medium Energy Beam Transport
MOSFET	Metal-Oxide-Semiconductor Field-Effect Transistor
NIEL	Non Ionizing Energy Loss
RFQ	Radio Frequency Quadrupole
SCR	Space Charge Region
SEE	Single Event Effect
SEL	Single Event Latch-up
SER	Soft Error Rate
STRAM	Software Tool for Radiation Absorption Maps
TID	Total Ionizing Dose

Introduction

In this chapter, the project will be motivated and described, and the contribution of the developed software tool will be presented. This introduction provides a qualitative idea of the thesis as well as an overview of the various chapters of the report, the latter is found in the thesis outline.

1.1 Motivation

Due to the radiatory environment in an accelerator, it is of great importance to study the radiation effects on electronics a priori the design of the electrical equipment layout. Furthermore, one must understand the limitations of such research. This is a necessity for making informed decisions regarding which candidate devices to use, where to locate them and, possibly, how to shield them. A device located at an unfavourable position may absorb a large quantity of radiation, causing data corruption and physical damage. These matters are crucial to account for in order to ensure that: data will not be corrupted, the up-time is maximized and the disposition of equipment is financially sustainable.

In order to withstand greater doses of radiation, radiation hard devices can be used. However, there are prevailing issues of radiation hardness calibration. The standard calibration is performed with ^{60}Co as a gamma source. ^{60}Co emits two energies of gamma radiation, 1.17 MeV and 1.33 MeV, which in this thesis is asserted to be insufficient for radiation hardness calibration. This issue is one of the great factors motivating the research presented throughout this thesis, and will be further discussed.

Furthermore, a software tool for mapping of radiation in terms of flux and energy spectra and its energy deposition in materials and devices is needed. This tool will be used for finding the magnitude of absorbed dose in electronics and materials.

1.2 Project specification

The main goal of the project is an assessment of the radiation impact on electronic equipment in the Front-End Building (FEB) of the European Spallation Source (ESS). The type of radiation of interest is ionizing gamma and neutron foremost,

however non-ionizing effects such as atom displacement is also discussed. It is desired to develop a tool to integrate the physical information from Monte Carlo radiation transport codes with the engineering requirements for electronics. The aim is to map, analyse and protect the electronic circuits against radiation in the accelerator tunnel of the ESS. To assess the radiation damage to electronics, it is necessary to calculate and simulate the neutron and gamma energy spectra and fluxes. Furthermore, the quantities used to predict radiation damage must be characterized and the energy spectra are to be folded with response functions of electronics and materials. This is a very important and complex issue. In this thesis, the focus must be put on a specific part of the accelerator. As the FEB will contain a large amount of electronics, this has been chosen as the main interest. However, the tools, analysis and understanding from this work will find applications in all radiatory environments. Furthermore, the magnitude of importance of this project is increased by the fact that there is a gap between experimental physicists and electronic engineers.

The primary challenge is to obtain a realistic radiation map of the area where one would like to install electronic equipment. At the ESS, Monte Carlo radiation transport codes are used to produce such maps. To input the correct parameters into the Monte Carlo codes, it is necessary to understand the physics of the accelerator and the processes creating neutrons. Insight in the microscopic processes known as nuclear reactions is needed as well as getting acquainted with the world of cross sections and interaction of radiation with matter.

The second challenge relates to electronic engineering. There are several physical processes that affect electrical circuits in radiation environments. This topic is very wide and it has applications extending beyond particle accelerators: from commercial aviation and satellites, to the International Space Station and the Mission to Mars. The objective in this regard is to understand the physics of the transistor and how it is affected by radiation. To achieve this, one must start from the p-n junction and the diode. Furthermore, the various errors that may occur in electronics due to radiation shall be studied and a certain focus must be chosen for this thesis.

The third challenge regards programming capabilities. It is desired to develop a tool that reads out maps of neutron and gamma fluxes, and spectra. This information shall then be folded with response functions for different types of electronic equipment and materials, thus providing a so-called *absorption map* revealing the absorbed dose of a device in a given environment. This map will be multidimensional, having three spatial coordinates, a scalar for the flux and a vector for energy spectra. The energy spectra in each point of the absorption map must be visualized in order to obtain sufficient arguments for whether a device location is favourable. The result of this is a tool that does not yet exist, however it is greatly desired.

There are, however, certain limitations, not the least in the understanding of radiation effects on electronics. Such limitations are explicitly addressed in Subsection 4.3.4.

1.3 Contributions

This report presents an investigation of radiation effects on electronics and sheds light on the prevailing issues regarding radiation hardness calibration. Particular interest is paid to the Metal–Oxide–Semiconductor Field–Effect Transistor (MOSFET), motivated by its presence in all digital equipment e.g. processors and memory devices. Furthermore, a novel software tool is developed for revealing the absorbed dose by electronics, thus being used for studying the possible damages to a device or material. The software demonstrates applicability in all areas where radiation is present. It can be used for any element, material or device for which a response function can be provided. The result of this software contributes to the possibility of a future global collaboration as every research facility may partake in the development of a library with electronics response functions. Such library would, in time, potentially aid every research facility within the field.

1.4 Thesis outline

Chapter 2 introduces the reader to the necessary background theory of elementary particles and nuclear reactions, with respect to the fundamental forces. The concept of cross sections is discussed and is of great importance for this project. Furthermore, physics of devices is discussed with particular interest in the transistor.

Chapter 3 presents the ESS and the concept of spallation. The linear accelerator is discussed with particular interest paid to the FEB.

Chapter 4 describes radiation and how it is interpreted when applied to humans with, a so-called, radiation weighting factor. Furthermore, the possibility applying a similar weighting factor to electronics is discussed. The various radiation effects and damages are presented and, finally, the current issues concerning radiation hardness calibration is discussed.

Chapter 5 explains how radiation simulations are connected to probability theory and the Central Limit Theorem, as well as cross sections and elementary particles. The simulation code is discussed, and establishes a fundament to the proceeding chapter.

Chapter 6 presents STRAM, a software tool developed in this project. The purpose of the tool is to read maps of particle fluxes and spectra, fold the information with response functions and produce a map revealing the expected absorbed dose of a studied material or device.

Chapter 7 presents an analysis and evaluation of the project objectives. Furthermore, the chapter summarizes the key content of the thesis and presents the final conclusions as well as a proposal for future work.

Appendices presents the code documentation of STRAM and an example of the numerical analysis method for automatic and accurate¹ rebinning of response functions. Also, empirical data provided by CERN, which is used for the construction of a response function for nitrogen compatible with STRAM, is presented. An example of radiation effects on cameras in particular is shown and, finally, an experiment guideline proposal for L.E.N.A facility in Italy is expressed.

¹Accurate – In this context this refers to rebinning of response function histograms, such that the new binning is designed to minimize the ∞ – *norm* of the error.

Prior to the project it is necessary to understand the physics of the accelerator and the processes creating neutrons. It is important to gain insight in nuclear reactions, cross sections and the Central Limit Theorem, and their connection to Monte Carlo methods.

2.1 Nuclear physics

2.1.1 Elementary particles and fundamental forces

In Figure 2.1, the standard model of all known elementary particles is shown. Furthermore, the figure shows the mass, charge and spin of the particles.

All matter is made from the particles in Figure 2.1, and held together by the fundamental forces presented in Table 2.1. To further investigate and understand the behaviour of the particles, the properties of quarks and antiquarks are presented in Table 2.3. The spin, charge, baryon number etc. are intrinsic properties of the particles. These properties determine the interaction with other particles. The fundamental forces of the universe and the Boson mediators consist of the following:

<u>Fundamental forces</u>	<u>Boson mediators</u>
Nuclear strong	gluons, g
Electromagnetism	photons, γ
Nuclear weak	$W(\pm 1)$, Z bosons
Gravitation	gravitons, G ²

Table 2.1: Fundamental forces and Boson mediators.

Note that everything that has mass, is influenced by gravitation, everything that has a charge is affected by electromagnetism and everything constructed by quarks is affected by the nuclear forces. An overview of the fundamental interactions can be seen in Table 2.2. Note that neutrons consist of one up and two down quarks whilst the protons consist of two up and one down quark.

²The graviton has not been observed.

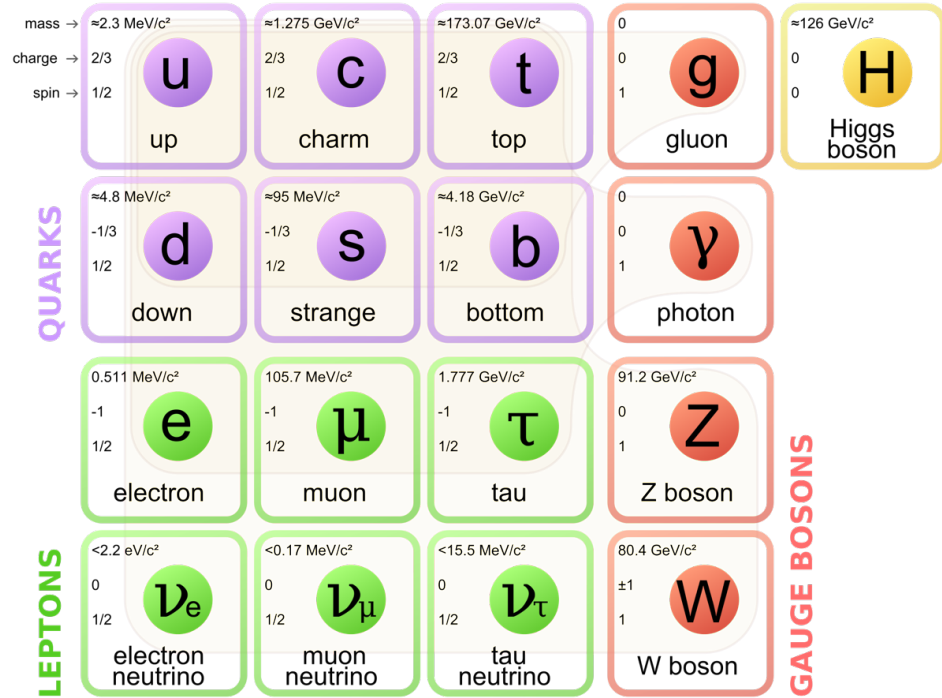


Figure 2.1: The standard model of elementary particles [1].

	Gravitation	Electro-magnetism	Nuclear weak	Nuclear strong
Protons, p^+	×	×	×	×
Neutrons, n^0	×		×	×
Electrons, e^-	×	×		

Table 2.2: Fundamental interactions.

To provide an intuitive idea of the various forces, consider a particle approaching a target. In layman's terms; depending on what forces the particle is affected by, which are found in Table 2.2, the particle will see the target differently. A proton will see the electromagnetic field as well as the nuclear forces of the nuclei. A neutron will see the considerably sparsely³ distributed forces of the nuclei only.

³Sparse – here: The fields of force with which a neutron interacts, can be considered sparsely distributed compared to the field experienced by a proton. A proton is influenced by the nuclear forces as well as the electromagnetic field which acts over potentially infinite distance as apposed to nuclear forces. Nuclear forces are powerfully attractive between nucleons at short distances compared to electromagnetism.

An electron, on the other hand, will see only the electromagnetic field. All three particles will, however, also be affected by gravity. In other words, the particles travel towards/through a target with different conditions. This will greatly affect the cross section for interactions as will be discussed in Subsection 2.1.3.

Flavor	Spin	Charge	Baryon number	Strange-ness	Charm	Truth	Beauty
Quarks							
u (up)	$\frac{1}{2}\hbar$	$+\frac{2}{3}e$	$+\frac{1}{3}$	0	0	0	0
d (down)	$\frac{1}{2}\hbar$	$-\frac{1}{3}e$	$+\frac{1}{3}$	0	0	0	0
s (strange)	$\frac{1}{2}\hbar$	$-\frac{1}{3}e$	$+\frac{1}{3}$	-1	0	0	0
c (charm)	$\frac{1}{2}\hbar$	$+\frac{2}{3}e$	$+\frac{1}{3}$	0	+1	0	0
t (truth)	$\frac{1}{2}\hbar$	$+\frac{2}{3}e$	$+\frac{1}{3}$	0	0	+1	0
b (beauty)	$\frac{1}{2}\hbar$	$-\frac{1}{3}e$	$+\frac{1}{3}$	0	0	0	+1
Anti-quarks							
\bar{u}	$\frac{1}{2}\hbar$	$+\frac{2}{3}e$	$+\frac{1}{3}$	0	0	0	0
\bar{d}	$\frac{1}{2}\hbar$	$+\frac{1}{3}e$	$-\frac{1}{3}$	0	0	0	0
\bar{s}	$\frac{1}{2}\hbar$	$+\frac{1}{3}e$	$-\frac{1}{3}$	+1	0	0	0
\bar{c}	$\frac{1}{2}\hbar$	$-\frac{2}{3}e$	$-\frac{1}{3}$	0	-1	0	0
\bar{t}	$\frac{1}{2}\hbar$	$-\frac{2}{3}e$	$-\frac{1}{3}$	0	0	-1	0
\bar{b}	$\frac{1}{2}\hbar$	$+\frac{1}{3}e$	$-\frac{1}{3}$	0	0	0	-1

Table 2.3: Properties of quarks and antiquarks [2].

2.1.2 Nuclear reactions

When a particle is incident on a nucleus, the incident particle may be scattered elastically or inelastically. There is also a chance that the particle is absorbed by the nucleus and other particles are emitted from the reaction. The so-called Q-value, is the value of the amount of released or absorbed energy from the reaction, where

$$Q = -(\Delta m)c^2 \quad [2] \quad (2.1)$$

If energy is released from a reaction, the reaction is said to be exothermic. In that case, the Q-value is positive. If, however, energy is needed for a reaction to occur, the reaction is called endothermic. This implies that the total mass of the outgoing particles is greater than that of the incoming particles and the Q-value is thus negative. The energy needed to start an endothermic reaction is slightly more than $|Q|$. This can be derived from the fact that Q is the binding energy of the target particles and the energy needed for an endothermic reaction is $Q + \epsilon_k$, where ϵ_k is a sufficiently large amount of energy for the outgoing particles to have kinetic energy enough to conserve momentum [2], [3].

2.1.3 Cross section

The Q-value is known for almost all possible nuclear reactions. However, the probability of the occurrence related to a given nuclear reaction is difficult to determine. The probability is used to identify how many reactions occur for any given time and volume.

The concept of cross section is quite complex. To get an intuitive idea, one may start by considering an analogy: When shooting at a target, the probability increases as the projectile and/or the target increases in size, or more correctly, when the largest cross section of the projectile and/or the target increases. With this analogy, the cross section can be described as

$$\sigma = \pi(R_p + R_t)^2 \quad [3] \quad (2.2)$$

where R_p and R_t are the geometrical cross section radii of the projectile and the target respectively.

Consider the arrow and the apple in Figure 2.2. In the top two figures, the projectile and the target can be seen. To determine the probability of hitting the target, we consider the cross section of the objects as seen in the bottom two figures. As mentioned, however, cross section is in reality far more complex. In the classical treatment, with the arrow and apple analogy, the cross section only depends on the geometrical area of the arrow head and the apple. Since nuclear reactions are governed by the laws of quantum mechanics, the geometrical cross section in equation 2.2, is replaced by the energy-dependent quantity

$$\sigma = \pi\lambda^2 \quad [3] \quad (2.3)$$

where λ is the de Broglie wavelength reflecting the wave aspect of quantum mechanical processes as

$$\lambda = \frac{m_p + m_t}{m_t} \frac{\hbar}{(2m_p E_l)^{1/2}} \quad [3] \quad (2.4)$$

where E_l is the laboratory energy of the incident projectile of mass m_p , m_t is the mass of the target nucleus and $\hbar = \frac{h}{2\pi}$ where h is Planck's constant. Nuclear charge and angular momentum may act to inhibit the penetration of the projectile into the nucleus, which implies strong energy dependence of the cross section. Furthermore, the cross section for a particular reaction depends on the nature of

the forces involved. It may depend on spin, charge and other potential attributes of the particle and nucleus involved.

As the cross section decreases, the challenge to empirically find σ increases vastly [2], [3].

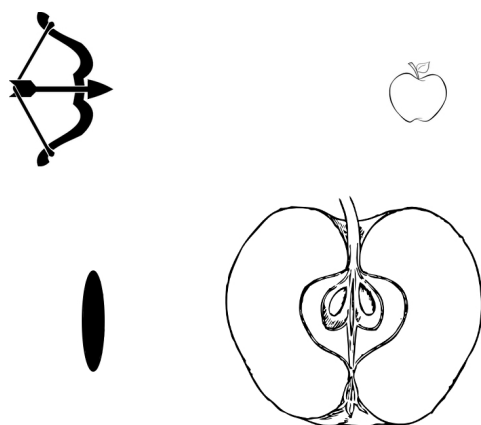


Figure 2.2: Arrow and apple cross section analogy.

2.2 Electronics and physics of devices

In order to understand radiation effects on electronics, particular interest is paid to the MOSFET throughout this project. The MOSFET is one of the most common and important components in embedded circuits for signal switching and power amplification. Digital integrated circuits such as microprocessors and memory devices can contain billions of MOSFETs. To provide sufficient insight in the physics of a MOSFET, this section presents the p-n junction, the diode and the bipolar junction transistor prior to the MOSFET.

2.2.1 p-n junction

To change the electrical properties of a semiconductor, impurities are intentionally introduced to the intrinsic material. This is performed with the purpose of obtaining semiconductors with the possibility of a p-n junction and is called doping. The p- and n-doping is a fundamental concept to comprehend for the overall understanding of modern electronics, not the least transistors. A p-n junction is the interface between a p- and n-doped material.

If a doping atom has more valence electrons than a host atom, then the doping atom will donate its extra valence electron to the conduction band. Therefore, the doping atom is called a donor. If a doping atom with less valence electrons than a host atom is introduced, the doping atom will accept an electron from the valence band of the host atom, thus leaving a hole in the valence band of the host atom. This type of doping atom is called acceptor. Doping with donors

implies the aforementioned n-doping, and doping with acceptors is called p-doping. Note that both an n- and p-doped material is neutral in itself, though electrons are majority charge carriers in the n-type material, whereas holes are majority charge carriers in p-type material. As shown in Figure 2.3, if a p-doped and n-doped semiconductor are put together, electrons and holes will recombine in the interface. Recombination causes the interface to lack free carriers and consists only of ionized doping atoms. This recombination is a consequence of electron concentration differences between the materials and it results in negatively charged acceptors and positively charged donors.

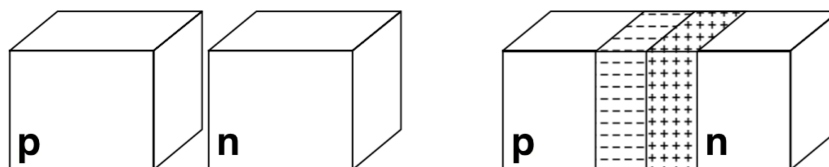


Figure 2.3: The figure shows how the electrons and holes in the interface of p-doped and n-doped materials recombine and create charged acceptors and donors [4].

The recombination causes a diffusion current. Just as a drift current can be formed by the electric field in a semiconductor, a diffusion current can be formed due to concentration differences of electrons and holes. The electrons move from the higher electron concentration towards the lower. If nothing prevents the electrons to distribute themselves evenly, the diffusion current will cease. In electrical components, such as the transistor, concentration differences are necessary for the component to work. This will be made clear in the following subsections.

The diffusion current is described by the concentration gradient, i.e. the derivative of electron concentration with respect to displacement $\frac{dn}{dx}$, which describes the reverse direction of the electrons as well as the magnitude of the current. The diffusion current is defined as

$$I_n = e \cdot A \cdot U_t \cdot \mu_n \cdot \frac{dn}{dx} \quad [4]$$

where e is the elementary charge, A is the cross section area in the p-n junction, U_t is the thermal voltage and μ_n is mobility of the electron in an electric field. The diffusion yields the current through a diode which is constructed with a p-n junction. The diode is presented in Subsection 2.2.2.

2.2.2 Diode

Consider two crystals, one p-doped and one n-doped both of which are homogeneously doped with the concentrations N_A and N_D respectively. As explained in Subsection 2.2.1, a p-n junction is obtained by putting together the two crystals as shown in Figure 2.3. Electrons move from n to p and holes move from p to n. Electrons and holes will recombine. If nothing were to prevent recombination, eventually, there would no longer be any free carriers in the interface and the

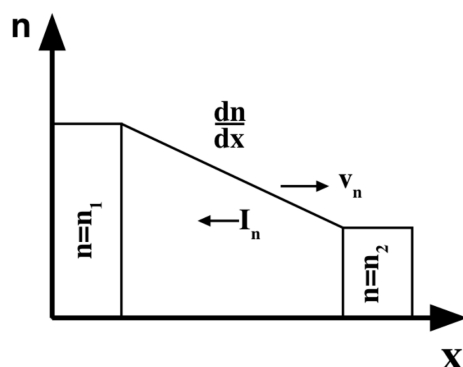


Figure 2.4: The figure presents the concentration gradient due to concentration differences between two reservoirs [4].

semiconductor would have homogenous charge distribution. However, as a donor donates an electron, the donor atom becomes positively charged and therefore attracts electrons from the rest of the n-doped material to the interface. The same goes for holes being created on the p-side, causing a negative charge. This negative charge will in fact prevent further electrons from moving from the n-side to the p-side. This works analogously for the holes on the p-side. At this point, a p- and n-doped area with free carriers are obtained, between which an area with ionized doping atoms fixed in the crystals are found. The areas with free carriers is of low resistance due to the mobility. However, the center area that has no free carriers is of high resistance. This center area is called the Space Charge Region (SCR). In other words, the SCR creates a barrier, preventing recombination of all electrons and holes.

Note that the space charge area strongly resembles a capacitor. The difference between the two concepts is that the SCR in a p-n junction is obtained by removing free carriers rather than adding them, which is the case for a capacitor. When the conductive plates of the capacitor is charged, a voltage is obtained across the plates. The same phenomenon appears for the SCR and is called internal potential and is a potential from the n-side to the p-side, i.e. positive to negative charge. If the potential over the p-n junction is less than the internal potential, the diode is said to be forward biased. If the potential over the p-n junction is greater than the internal potential, the diode is said to be reverse biased. When a diode is forward biased, the current increases exponentially with the applied voltage whereas the current is constant, and markedly smaller, when the diode is reverse biased. This is illustrated in Figure 2.5. In the ideal case, the current of a reverse biased diode is defined by the gradient of the majority charge carriers on the low-doped side. As this is constant, the current is also constant. Note that this is not true for any voltage, however this will not be important during this discussions.

Consider now an external voltage across a conductor. This implies that the charge on the plates is increased by supply of free carriers. For a p-n junction, however, free carriers must be removed to cause the charge and thus, the SCR increases. This means that the resistance increases as shown in Figure 2.5.

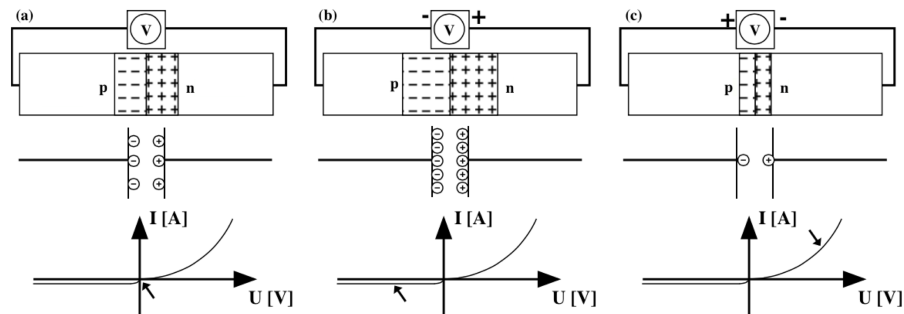


Figure 2.5: The figures illustrate how applied voltage changes the SCR. In figure a) no voltage is applied, the diode in figure b) is reverse biased, yielding a larger SCR and the diode in figure c) is forward biased, thus decreasing the SCR. [4]

2.2.3 Photodiode

The purpose of the photodiode is to transform light into current. When a photon strikes a diode with an energy $E_\gamma \geq E_{bandgap}$, where $E_{bandgap}$ is the energy needed to excite a valence electron in the diode, an electron will be excited from the valence band to the conduction band. When this occurs, a free electron is generated in the conduction band and a free hole is generated in the valence band. If a sufficient number of photons are absorbed, then enough free charge carriers are generated in order to change the conductivity of a diode.

Note that, when free electrons are generated on the neutral p-side in the diode, they will not move in a definite direction rather than randomly. At some point, corresponding to the lifetime of the free electron, it will recombine with a hole. This implies that no net current is obtained. Analogously, no net current will be obtained when free electrons are generated on the neutral n-side. The current in a photodiode occurs when free charge carriers are generated in the SCR and driven by the electrical field caused by the internal potential. When this occurs, electrons move towards the n-side and holes towards the p-side.

There is in fact a certain probability that a randomly moving charge carrier generated on the neutral n- or p-side may enter the SCR. However, this is merely a minor contribution to the current generated by electron generation in the SCR.

The minimum energy needed for the photon to be absorbed and an electron to be excited to the conduction band is the energy of the band gap, i.e. $E_\gamma = E_{bandgap}$. If a photon is not absorbed, it may pass through the diode without interaction or be reflected at the surface. A photon with $E_\gamma \geq 2E_{bandgap}$, may excite two electrons, though this is often neglected due to the improbable nature.

Note that a photon with $E_\gamma \geq E_{bandgap}$ is a necessary, yet not sufficient, condition for the photon to be absorbed. A photon interacting with an electron can only be described as a probability and is determined by the cross section for a photon to be absorbed by an electron. However, it is of great relevance to consider the quantum efficiency $\eta(0 \leq \eta \leq 1)$. The quantum efficiency is

defined as the probability of an incident photon to generate a free electron-hole pair that contributes to a current through the diode, i.e. that do not recombine. In a radiatory environment the quantum efficiency can be considered as the ratio of the flux of generated electron-hole pairs contributing to current through the diode, to the flux of incident photons. The quantum efficiency can be written as

$$\eta = (1 - \mathcal{R})\zeta[1 - \exp(-\alpha d)] \quad [5]$$

where \mathcal{R} is the optical power reflectance at the surface, ζ is the fraction of electron-hole pairs that contribute to current through a diode, α is the absorption coefficient of the material (cm^{-1}) and d is the depth of the diode, see Figure 2.6.

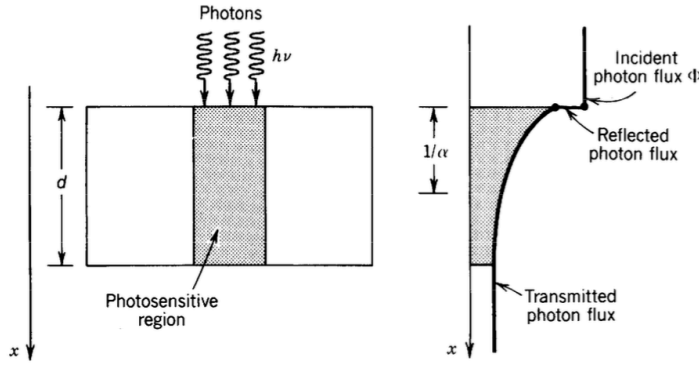


Figure 2.6: The figure depicts the effect of absorption on the quantum efficiency η ($h\nu$ is the energy of the incident photon, with the notation used in [5]).

Note that the term $1 - \mathcal{R}$ represents the effect of reflection at the surface of the diode and $1 - \exp(-\alpha d)$ represents the fraction of the photon flux that is absorbed in the bulk of the material. [4], [5]

The geometry and doping of a photodiode is designed such that it optimizes the absorption. This is of course not the case for the diodes in a transistor, however the physics is the same and absorption is yet occurring. When absorption occurs in a transistor, e.g. in embedded circuits, it may result in undesired consequences such as corrupted data or device malfunction. Such errors will be discussed in Chapter 4.

2.2.4 Bipolar junction transistor

A transistor is a widely used semiconductor device, used for power amplification and signal switching. It is one of the most essential and common active components in electronics and therefore of great interest within research of radiation effects on electronics.

The Bipolar Junction Transistor (BJT) is a p- and n-doped semiconductor component. It has a thin layer of one type of doping in the centre, with material of the other type of doping on each side, as presented in Figure 2.7. The three

regions of the BJT are called emitter, base and collector. The BJT works in such a way, that a small current through the base brings a larger current through the collector and the sum of the currents exits through the emitter.

Consider two crystals with an asymmetrical junction where $N_D \gg N_A$, i.e. the concentration of donors on the n-side is much higher than the concentration of acceptors on the p-side. This is often referred to as an n^+p junction or n^+p diode. In order for a current to go through a forward biased diode, and not only within the SCR, electrons need to be injected by drift current on the n-side. The drift current causes the electrons to move from the electrode on the n-side to the SCR. In the SCR, diffusion current and drift current work in opposite directions, the diffusion current being the stronger, forces the electrons over to the p-side. The diffusion current causes the electrons to move across the p-side to the electrode and finally drift current transports the electrons through the electrode to the positive terminal of the source.

Now consider the BJT as presented in Figure 2.7 which may be examined as two parts, the forward biased base-emitter diode and the reverse biased base-collector diode.

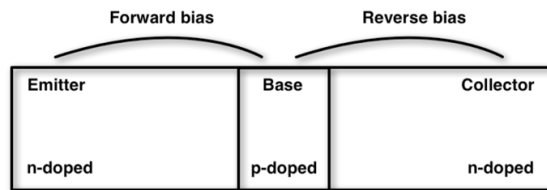


Figure 2.7: The bipolar junction transistor (BJT) consists of three doped regions. The base-emitter is forward biased and the base-collector is reverse biased.

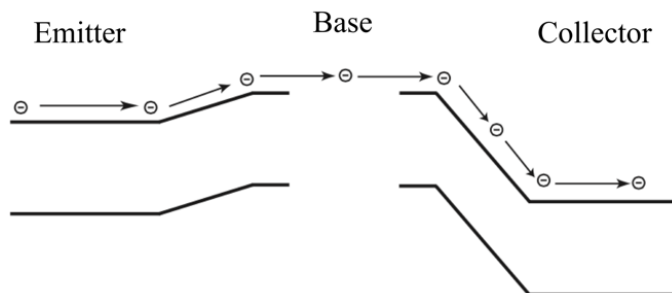


Figure 2.8: The figure shows the idea of how a forward biased diode is used to move electrons to the SCR of a reverse biased diode. The forward biased diode, base-emitter, works as an electron generator and the reverse biased diode, base-collector, collects the electrons. [4]

Electrons move from the n-side of the forward biased diode in Figure 2.7, to the SCR of the reverse biased diode and finally to the n-side of the reverse biased diode. As the current is defined in the opposite direction of the electrons, the current moves from the collector to the emitter.

Now recall the aforementioned n^+p -diode. The concentration of donors on the n-side is much greater than the concentration of acceptors on the p-side, i.e. the electron current is much greater than the hole current and the hole current may therefore be neglected. Consider two n^+p -diodes constructing a BJT. A large electron current flows through the collector and a minor hole current flows through the base, the latter being negligible. The current flowing through the emitter is the sum of the two former currents, approximately with the magnitude of the collector current.

It is now possible to draw the conclusion that a minor current through the base will consequently cause a large current through the collector and thus a large current out of the emitter. This is very beneficial as the base current can be controlled, which in its essence yields the ability to control and amplify the emitter current. However, in order to use this amplification, sufficient power must be supplied to the collector. The ability to control and amplify the emitter current is the very essence of the component which has hereby been described.

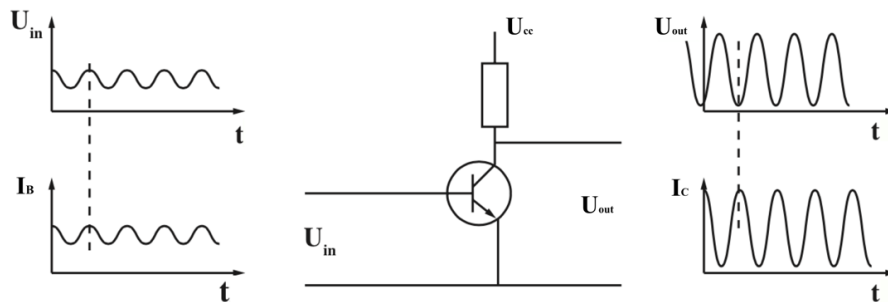


Figure 2.9: The figure illustrates the amplification of an input signal on the base of a BJT, given a sufficient voltage, U_{cc} from a power supply [4].

2.2.5 MOSFET

In this report, focus will be put on the MOSFET. As the name suggests, the MOSFET consists of a semiconductor with an oxide-surface, which has a metal connection on top. In its essence, it resembles a capacitor with one plate made of metal and one plate made of a semiconductor, with oxide insulation in between. The MOSFET commonly handles very small currents and voltages. They are usually embedded in digital circuits, where small currents are desired to minimize the energy consumption.

For an explanatory comparison, consider the capacitor. A voltage over the capacitor will yield a positive charge on the plate connected to the positive side of

the source, and a negative charge on the negative side of the source. Analogously, a positive voltage over a p-type semiconductor yields a positive charge on the surface, i.e. an increased hole concentration. This is called accumulation. A negative voltage implies a negative charge caused by repulsion of holes and the surface thus consists of ionized acceptors, as in the SCR of a diode. However, the acceptors are immobile and thus causes resistance close to the surface of the p-substrate, while a negative charge consisting of free electrons would give rise to inversion. Inversion implies an inversion of charge carriers. A sufficiently large voltage yields more electrons than holes on the surface and the p-type has been inverted to n-type. A layer of inverted charge carrier concentration is obtained and the layer in proximity to the surface is called inversion channel. This is illustrated in Figure 2.10. As the charge carrier type is inverted at the surface, a p-substrate MOSFET is called n-MOS, and vice versa for n-substrate MOSFET.

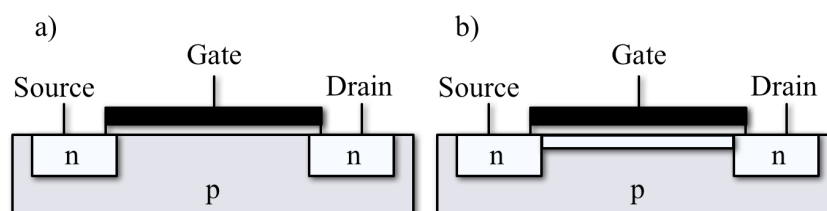


Figure 2.10: In figure a), a cross section of a MOSFET without applied voltage is seen. In b), a sufficient voltage is applied, yielding an inversion channel between the source and the drain.

Charge carriers are supplied to the source, the gate creates the inversion channel and the charge carriers are extracted from the drain. When no voltage is supplied, the transistor in Figure 2.10 resembles a BJT. The most significant difference is that the distance between the n-doped materials is larger in the MOSFET. This implies that it is in fact two opposing diodes, meaning that no current is flowing through an inversion channel in either direction as a reverse biased diode will be seen in both directions. If a sufficiently large voltage is applied on the gate, however, the gate will generate an inversion channel allowing free electrons to pass between source and drain. At this point, a voltage over source and drain will yield a source-drain current. The smallest voltage necessary for the gate to generate an inversion channel is called threshold voltage.

For the purpose of investigating radiation effects on electronics, the inversion channel, in particular, is of great interest. Recall the discussion in Subsection 2.2.2, explaining that the current of a reverse biased diode is defined by the concentration gradient of charge carriers. A larger gradient implies a larger current. In a MOSFET, the current is given by the voltage difference between source and drain, and the resistance in the inversion channel. This current is a drift current. For low source-drain voltages, the current is increasing seemingly linearly as the voltage increases as seen in Figure 2.11. Note that no current is flowing through the gate, as apposed to the BJT.

The digital switching of a MOSFET depends on the inversion channel. When

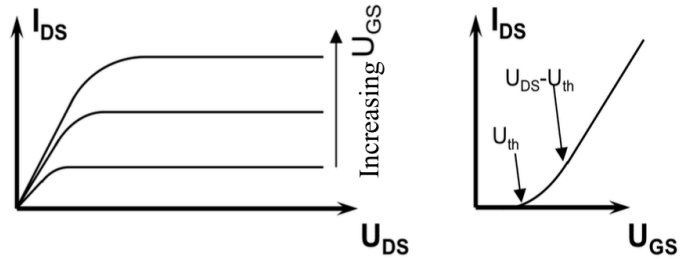


Figure 2.11: The figure illustrates how the drain-source current depends on drain-source voltage and gate-source voltage [4].

an inversion channel is present, a drift current flows between source and drain. In digital circuits, this is defined as 1 and otherwise it is defined as 0. As the digital data consists of these zeros and ones, the data will be corrupt if there is an undesired switch flip, or bit flip if you will. This can occur through various radiation related phenomena. This background theory is important for further discussions in Section 4.3, where the radiation effects on electronics are presented. [4]

For the purpose of understanding the coupling of the theory hitherto discussed and its application at the ESS, it is preferable to provide some insight in the various parts of the accelerator prior to the presentation of radiation and its effects of electronics. Particular attention has been given to the FEB, which is presented in Subsection 3.2.1.

3.1 Spallation

Spallation is the process where a heavy nucleus emits particles, including neutrons, after being hit by a high energy particle.

At the ESS, this is achieved by means of a particle accelerator and a heavy metal target. Protons are derived from hydrogen and are accelerated close to the speed of light⁴, from 75 keV to 2 GeV, in the linear accelerator tunnel under vacuum. At the end of the accelerator tunnel, the monolith is located. The proton beam passes a so-called Proton Beam Window, which separates the high vacuum of the accelerator beam tube from the helium atmosphere in the monolith. The proton beam then collides with a flat cylinder target wheel made of tungsten. The collision between protons and nuclei of the target will consequently scatter a collection of high-energy neutrons in all directions.

Scattered neutrons enter the moderator and reflector system consisting of 20 K parahydrogen⁵ moderators, inside an inner reflector of beryllium. These components will be kept at their desired operational temperature by dedicated cooling systems. The moderators are vessels with liquid parahydrogen for slowing down the high-energy neutrons. When a high-energy neutron collides with a proton, momentum is transferred from the neutron to the proton causing the velocity of the neutron to decrease and the velocity of the proton increase. However, as the proton is affected by electromagnetic interactions, as opposed to the neutron, the proton

⁴Protons are accelerated to approximately 90% of the speed of light

⁵Parahydrogen possesses particular attributes in terms of spin. As opposed to orthohydrogen, the proton spins of parahydrogen are aligned antiparallel. When a neutron collides with the parahydrogen, the neutron transfers momentum to the proton and deposits further energy to convert the parahydrogen into orthohydrogen. Through this phenomenon, parahydrogen can more efficiently moderate the neutrons.

will quickly lose energy and thus the moderator and reflector system remains very efficient and stable.

The reason for hydrogen to be the element of choice in the moderator, is the fact that the mass of neutrons and of protons are nearly the same. Consequently, the neutron can pass almost all its energy to a proton. However, the absorption cross section is very low, thus the risk for the neutron to die is very small.

The scattered neutrons can exit the moderator system through, up to, 48 beam ports. This way, the stream of neutrons is directed towards an array of scientific instruments. Each of these instrument stations is uniquely calibrated to observe a different set of interactions between the neutron beam and the material or tissue sample the experiment is designed to analyse.

The more neutrons that are obtained, the better the resolution of the results will be obtained. The phenomena to observe is in fact the neutrons' interaction with the studied material or tissue. One may investigate how the neutrons collide with the sample, how they pass through it or how they interact with, for example, the electromagnetism present in the sample. [6] [7]

3.2 Linear accelerator

A simple schematic of the accelerator is presented in Figure 3.1. The red colour coding represents the normal conducting linear accelerator, or "linac" as it is often called. The blue represents the superconducting linac and finally, the target is seen in the circular block.

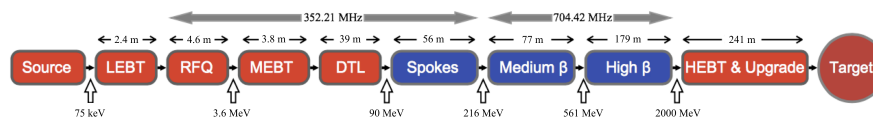


Figure 3.1: Updated block diagram of the linear accelerator presented in the Technical Design Report in [7].

3.2.1 Front-End Building

A software tool is developed in this project as mentioned in the project specification in Section 1.2. The tool's application at the ESS is demonstrated primarily in the FEB. Therefore, the various sections of the accelerator in the FEB is of particular interest in this report. Note however, that the radiation in the FEB depends not only on the accelerator sections in the FEB. Much of the radiation in the FEB is contributed by the Drift Tube Linac (DTL), which is the first section in the accelerator tunnel, i.e. after the FEB. In fact, through simulations it has been shown that about 80% of the radiation in the FEB is contributed by the DTL. The FEB has an underground housing for the ion source, Low Energy Beam Transport (LEBT), Radio Frequency Quadrupole (RFQ), and the Medium Energy Beam Transport (MEBT).

The normal conducting accelerator, represented in red colour in Figure 3.1, is also called the warm linac. This is where protons are created and accelerated to 90 MeV. The first section is the Electron Cyclotron Resonance Ion Source, i.e. the source. In the source, hydrogen plasma is produced by superimposition of the electrons with a high frequency electromagnetic wave at the electron cyclotron resonance frequency. The interaction generates hot electrons, which are then able to ionize the atoms. The ESS proton source design merges several solutions with a flexible magnetic system to produce magnetic profiles of higher currents and proton fractions [7].

The proton beam created in the source enters the LEBT. In the LEBT, the beam is further focused and chopped with sharp flanks to prevent the beam from continuing in the linac before the source output has stabilised. The focused and chopped beam then enters the RFQ where the beam is accelerated to 3.6 MeV. Next, the beam enters the MEBT, which has four functions:

1. Use optics to steer the beam from the RFQ to the DTL.
2. Use beam instrumentation to obtain information about the condition and location of the beam.
3. Collimate the beam.
4. Chop the beam (faster than the LEBT chopper).

The radiation in the FEB largely consists of neutrons and gammas and, through simulations results it has been determined that other particles are negligible.

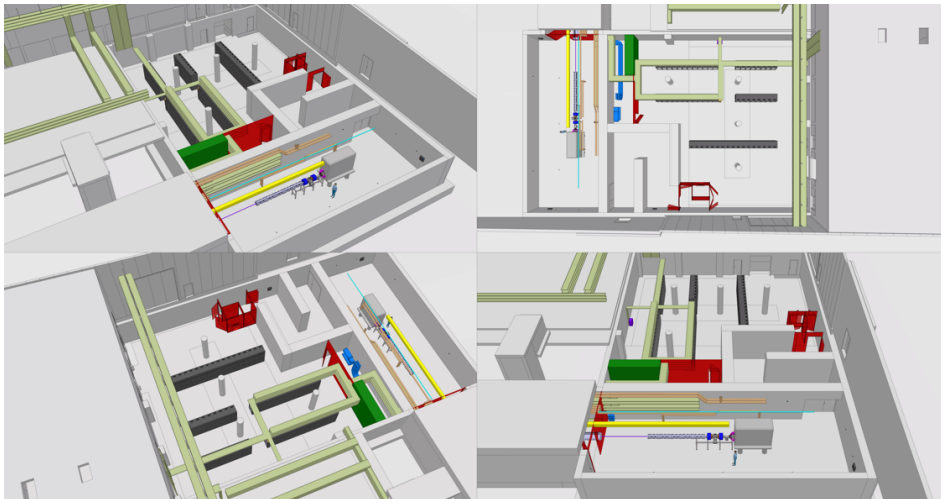


Figure 3.2: Preliminary schematics of the front-end building of the ESS [8] [9].

An open discussion at the ESS regards the desire of locating cameras in the FEB. The manifestation of possible radiation effects on cameras can be seen in Appendix D.

3.2.2 Accelerator tunnel

After the MEBT, the beam exits the FEB and enters the tunnel. First, the DTL is entered. In the DTL, the protons are accelerated to approximately 90 MeV. The beam then enters the superconducting linac, which is colour coded in blue in Figure 3.1. In the three superconducting niobium cavities, operating at a nominal temperature of 2K, the protons are accelerated from 90 MeV to 2 GeV. First off is the Spoke section consisting of 14 double-spoke cavities in 14 cryomodules with superfluid helium cooling provided by the cryogenic system. The niobium cavities resonate at a frequency of 352.21 MHz, and the electromagnetic field accelerates the protons to 216 MeV. The next section, Medium- β , consists of elliptical cavities with four five-cell cavities per cryomodule, accelerating the protons to 561 MeV. This is followed by the high- β of the same concept, which accelerates the protons to 2 GeV. The last part of the tunnel is the High Energy Beam Transport (HEBT), which transports the beam to the target at approximately 90% of the speed of light. [6] [7]

3.2.3 Target station

The main function of the target station is to convert high-energy proton beam from the accelerator into low-energy neutron beams with the greatest possible efficiency, safety and reliability. There are three groups of target station subsystems⁶ [6] [7]:

1. **Target monolith and associated subsystems** interact directly with protons and/or neutrons. It includes:
 - **The proton beam window**, which separates the high vacuum in the accelerator from the atmospheric-pressure inert helium gas inside a large vessel in which all of these systems are housed. They form, together with the tight container, the target monolith, which takes the shape of a 12 m diameter and 10 m high cylinder.
 - **The rotating target wheel system**, which is a rotating tungsten wheel as earlier mentioned. It distributes the irradiation over a large volume of target material. After periods of operation, the target emits significant amount of after-heat, gradually decaying in time.
 - **The moderator-reflector assembly**, which surrounds the target and will transform the fast neutrons into slow neutrons and thus making them useful for research. The ESS target station will contain two liquid-hydrogen moderators with a volume of about 2.5 l each, partially surrounded by water pre-moderators. The moderators are placed inside an inner reflector of about 1 m³ of beryllium. These components will be kept at their desired operational temperature by dedicated cooling systems. These systems will not emit significant after-heat.

⁶Caveat – The information presented in this subsection is based on the preliminary design presented in the Technical Design Report in [7]. Several of the design choices may change prior to the construction.

-
- **The beam extraction system**, which guides the slow neutrons to neutron scattering experimentalists. The beam-extraction system will consist of more than 40 beam tubes arranged in four sectors with a 60° to 65° horizontal angular spread. Each beam tube will be equipped with a beam shutter within the target monolith. The beam shutters assure that the residual radiation escaping through the closed beam line is reduced to safe working levels at the wall of the target monolith, when the target station is not in operation. The monolith will be surrounded by a combination of integrated and individual radiation shielding for each beam line. This is to guarantee safe working access to the areas outside of these shielding structures all the time, including during full power operation.
2. **Fluid systems** including the closed cooling circuits and the radioactive gaseous effluents and confinement system.
 3. **Handing and logistics subsystem** includes active cells, caskets and remote handling systems. These subsystems transport, exchange, maintain, process, package, store and release the used radioactive components from the target station operation.

Radiation and its connection to matter is discussed throughout this chapter. This thesis sheds light on gamma and neutron radiation foremost though particles as muons, betas, and alphas are also mentioned. Furthermore, a parallel between radiation effects on human tissue and on electronics is presented in this chapter. Finally, the issues of radiation hardness calibration is discussed.

4.1 Radiation effects on human tissue

Regarding glossary in the area of radiation, the Compendium of Dose Coefficients by ICRP states many useful terms. Several of these terms regard radiation exposure to human tissue and, interestingly, there is a radiation weighting factor. This factor serves the purpose of providing an estimate of the radiation damage on human tissue. In other words, the value of any given dose is modified depending on the type, and in some cases the energy, of the incident particle. Such weighting factor will later be discussed and motivated to be a possible approach even for electronics:

“Absorbed dose (D)

The physical dose quantity given by $D = \frac{d\bar{\epsilon}}{dm}$ where $d\bar{\epsilon}$ is the mean energy imparted by ionising radiation to matter in a volume element, and dm is the mass of matter in this volume element. The SI unit for absorbed dose is joule per kilogram (J/kg) and its special name is gray (Gy).

Committed effective dose [$E(\tau)$]

The sum of the products of the committed organ or tissue equivalent doses and the appropriate organ or tissue weighting factors (w_T), where τ is the integration time in years following the intake...

Committed equivalent dose [$H_T(\tau)$]

The time integral of the equivalent dose rate in organ or tissue T that will be received by an individual following intake of radioactive material into the body, where τ is the integration time in years following the intake...

Effective dose (E)

The sum of the weighted equivalent doses in all tissues and organs of the body, given by the expression $E = \sum_T w_T H_T$, where H_T is the equivalent dose in organ or tissue T , and w_T is the weighting factor for tissue T .

Equivalent dose (H_T)

The equivalent dose, $H_{T,R}$, in tissue or organ T due to radiation R , is given by $H_{T,R} = w_R D_{T,R}$ where $D_{T,R}$ is the average absorbed dose from radiation R in tissue T and w_R is the radiation weighting factor. Since w_R is dimensionless, the units are the same as for absorbed dose (J/kg) and its special name is Sievert (Sv). The total equivalent dose H_T is the sum of $H_{T,R}$ over all radiation types: $H_T = \sum_R H_{T,R}$.

Kerma (K)

The quotient of dE_{tr} by dm , where dE_{tr} is the sum of the initial kinetic energies of all the charged ionising particles liberated by uncharged ionising particles in a volume element of mass dm , thus $K = \frac{dE_{tr}}{dm} \dots$

Radiation weighting factor (w_R)

The radiation weighting factor is a dimensionless factor to derive the equivalent dose from the absorbed dose averaged over a tissue or organ, and is based on the quality of the radiation.” [10]

4.2 Radiation weighting factors

Regarding the equivalent dose H_T , the weighting factors for tissue, w_T , there is a certain inconsistency between different publications.

In the Swedish Radiation Safety Authority (SSM)⁷ Regulatory Code [11], the weighting factors somewhat differ from the same authority’s special conditions for the ESS facility in Lund [12] as seen in Tables 4.1 and 4.2. In fact, they both differ from the statements of ICRP in [13], whose results can be seen in Table 4.3.

Radiation type & energy	w_R
γ, β, μ	1
n , E(MeV)	$5 + 17e^{-\frac{(\ln(2E))^2}{6}}$
p , except recoil protons, $E > 2MeV$	5
α nuclear fission products heavy nuclei	20

Table 4.1: Weighting factors for radiation from the SSM Regulatory Code [11].

⁷SSM – Strålsäkerhetsmyndighetens

A graph depicting the three different radiation weighting factors for neutrons is shown in Figure 4.1. SSM's regulatory code is a smooth function whilst their special conditions for the ESS consists of three functions which seem to have non-smooth handshakes. In fact, by analysing the formulas in the points of handshake, the following results are found:

$$E = 1MeV \Rightarrow \begin{cases} \frac{d}{dE}(2.5 + 18.2e^{-\frac{(\ln(E))^2}{6}}) = 0.000 \\ \frac{d}{dE}(5.0 + 17.0e^{-\frac{(\ln(2E))^2}{6}}) = -3.626 \end{cases}$$

$$E = 50MeV \Rightarrow \begin{cases} \frac{d}{dE}(5.0 + 17.0e^{-\frac{(\ln(2E))^2}{6}}) = -0.015 \\ \frac{d}{dE}(2.5 + 3.25e^{-\frac{(\ln(0.04E))^2}{6}}) = -0.014 \end{cases}$$

As seen in the first handshake, i.e. at $E=1$ MeV, there is quite the difference in the gradient of the handshake point. The gradients in the second point of handshake, $E=50$ MeV, are not as different, yet not identical.

Radiation type & energy	w_R
γ, β	1
$n E_n < 1MeV$	$2.5 + 18.2e^{-\frac{(\ln(E))^2}{6}}$
$n 1MeV < E_n < 50MeV$	$5.0 + 17.0e^{-\frac{(\ln(2E))^2}{6}}$
$n E_n > 50MeV$	$2.5 + 3.25e^{-\frac{(\ln(0.04E))^2}{6}}$
$p, \text{ charged } \pi$	2
α	20

Table 4.2: Weighting factors for radiation from the SSM's special conditions for the ESS facility in Lund [12].

A similar weighting factor may be very desirable for electronics. This matter is motivated and shortly discussed in Section 7.1.

Radiation	Energy	w_R
γ, β, μ		1
n	$< 10keV$	5
	$10keV - 100keV$	10
	$100keV < E_n < 2MeV$	20
	$2MeV < E_n < 20MeV$	10
	$> 20MeV$	5
p , other than recoil, $> 2MeV$		5
α nuclear fission products heavy nuclei		20

Table 4.3: Weighting factors for radiation from ICRP Publication 60 [13].

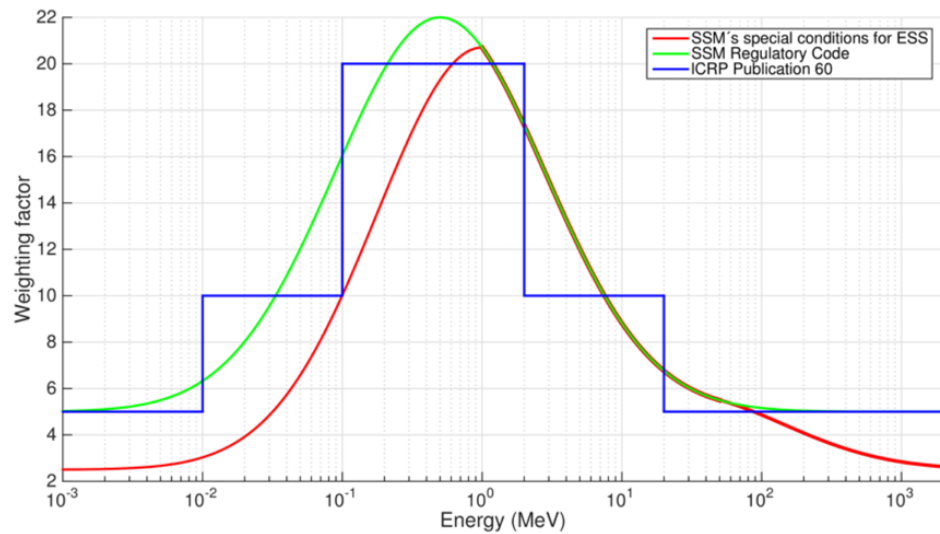


Figure 4.1: Radiation weighting factors for neutrons.

4.3 Radiation effects on electronics

Radiation effects on electronics can be divided into two main categories, cumulative effects and Single Event Effects (SEE). In this section, the weight will be put

on cumulative effects, particularly Total Ionizing Dose (TID). TID is of great importance in this report as it connects much to the MOSFET, which has been thoroughly studied as it is found in all digital circuits.

4.3.1 Cumulative Effects

This type of effects build up over time and do not manifest any symptoms until the accumulation of affecting events are sufficiently severe. There are mainly two types of cumulative effects, the aforementioned TID and Non Ionizing Energy Loss (NIEL).

TID may cause a shift of threshold voltage in MOSFETs due to trapped charges in the SiO_2 gate insulator. Recall the MOSFET in Subsection 2.2.5. When high energy particles strikes the transistor substrate, a shower of particles scatter causing ionization. This can lead to charges being trapped in the SiO_2 gate insulator. Furthermore, if SiO_2 -bindings are broken by photons, the SiO_2 becomes ionized and again, charges can be found in the insulator. These charges shift the threshold voltage U_{th} . The trapped charges may also generate an inversion channel, thus causing a drift current I_{DS} . In this event, the digital signal will be 1 regardless of the desired signal and the data will therefore be corrupt. In other words, the characteristics of the transistor may be changed and thus become unreliable.

The trapped charges can escape by tunnelling effects, i.e. the charges may pass through the barriers, causing increased leakage and thus increased power consumption. Tunnelling is a quantum phenomena where a particle penetrates and, often, passes through a potential barrier which is greater than the kinetic energy of the particle. This is not allowed by the laws of classical dynamics and is related to the treatment of matter in quantum mechanics where the matter is considered having properties of both waves and particles. This involves the Heisenberg uncertainty principle, which asserts a limit to the precision with which certain complementary pairs of physical properties of a particle can be known simultaneously⁸ [15]. This complex phenomena indeed provides further difficulties with predicting the various radiation effects on a device.

The severity of the effect from trapped charges depends much on the geometry of the transistor. The greater the volume of the SiO_2 -layer, the more charges can be trapped. Though it is difficult to generalize the different geometries, it may be possible so obtain a sufficient understanding of a transistor's tolerance. In other words, it may be possible to determine whether relocation, shielding or other measures are necessary for a transistor, let alone a device, in order to survive in a given environment.

A MOSFET's sensitivity to TID is strongly related to technology and manufacturing process along with many more dependencies stated in Subsection 4.3.4, *Limitations*. Therefore, a simplified model for accurate predictions of TID effects is not available [16].

NIEL occurs mainly due to accumulation of displacement damage in the lattice. Hadrons may displace atoms in the silicon lattice and affect their function. The

⁸Tunnelling is thoroughly explained in [14].

substrate layer in proximity to the SiO_2 , i.e. where the inversion channel is created, may be damaged by irradiation which causes a decrease in transconductance and thus a decreased drift current. Over time the integrated flux, also known as the fluence, may cause severe displacement damage and even destruction. [17] [18] [19] [20]

Figure 4.2 shows how ionizing radiation generate electron-hole pairs in the oxide of a MOSFET. The electrons move toward the gate and the holes move toward the substrate. The holes generated in the oxide eventually encounter a distribution of hole traps. These traps are assumed to start at the Si/SiO_2 interface and extend 5 to 10nm into the oxide. “Depending upon the local density, N_{ht} , and hole capture cross section, σ_{ht} , of the hole traps, a fraction of the holes incident on the trap distribution are captured. The remainder continue into the Si and are recombined. Those holes that are captured by hole traps within a certain distance of the Si are assumed to be rapidly removed by electrons tunnelling from the Si , and therefore these traps are effectively empty or non-existent as far as ΔV_{ot} is concerned. This process is believed to be largely responsible for the ‘long-term annealing’ of ΔV_{ot} . ΔV_{ot} being trapped positive oxide charge. [21]

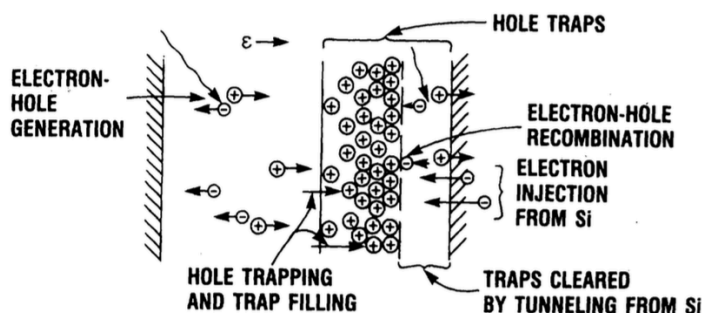


Figure 4.2: The figure illustrates how ionizing radiation generate electron-hole pairs in the oxide [21].

4.3.2 Single Event Effects

Though the main focus regarding radiation effects is put on cumulative effects, SEEs are preferably mentioned. This is preferred for the sake of a wider understanding of radiation effects on electronics.

If a particle is highly ionizing, it may deposit an amount of charge in the silicon sufficient for disturbing the function of the circuit. As this is caused by direct ionization, it is called Single Event Effects. As this is a single event, it can only be characterized in terms of the probability for occurrence. Furthermore, a distinction must be made between destructive and non-destructive SEEs. Soft SEEs refer to recoverable non-destructive effects, namely:

- Single Event Upset: If an ion with sufficient energy strikes near a transistor in a memory cell, the deposited charge may cause a bit flip.

- Multiple Bit Upset (MBU): MBU is a soft error resulting from an ion striking a memory circuit with sufficient energy to cause bit flips in several cells.
- Single Event Transient (SET): SET occurs when an ion strike causes a brief voltage spike at the node of a circuit and creates a transient in the circuit. If the transient propagates and becomes latched in the circuit, it may lead to single event upset.
- Single Event Functional Interrupt (SEFI): SEFIs do not depend on a single cause, hence it is quite cautiously defined. However, SEFIs are observed in microcircuits though with statistically low probability compared to other SEEs.

Hard SEEs refer to non-recoverable destructive effects, namely:

- Single Event Latch-up (SEL): SEL is a hard error where particle strike deposits enough charge to cause abnormally high currents and a short circuit between power supply and ground. This results in function loss of the device until the device is reset. An SEL may be destructive if the current causes sufficient thermal damage.
- Single Event Gate Rupture (SEGR): An SEGR is a breakdown and subsequent conducting path through the gate oxide of a MOSFET. This may be caused by a single high energy particle strike. SEGR is manifested by an increase in gate leakage current and can result in either the degradation or the complete failure of the device.
- Single Event Burnout: Destructive switching failure in power MOSFETs caused by localized high current. [17] [18] [19] [20]

With the purpose of further examination in a hands-on manner, several experiments were performed in this project. The experiments took place at Nuclear Physics, Physics Department, Lund University. In the first experiment, a Spark-Fun Logomatic Data Logger was used to log zeros over a given time. This was performed simply by connecting the ground to the logged port. In the second experiment, the circuit was irradiated by a neutron source, which may not be disclosed in this report, with a flux of $\Phi = 1.1 \cdot 10^7 ns^{-1} cm^{-2}$ isotropically, and energies around 5 MeV. Both experiments were repeated twice. The results were analysed with MATLAB, however no SEEs could be determined with certainty. A noteworthy conclusion may nevertheless be that the energies and flux was insufficient for the assessment of generating SEEs in the circuit.

4.3.3 Neutron induced soft errors

Although the focus is aimed mainly at cumulative effects, an idea of neutron induced soft errors is of great value as it will aid the overall understanding of radiation effects on electronics. Furthermore, this subsection will later on connect to the current issues with ^{60}Co calibration of radiation hard devices. This will be further discussed in Subsection 4.3.5.

In [22], soft errors in MOSFETs from 25 nm to 65 nm design rule were analysed with Monte Carlo simulation using PHITS⁹-HyENEXSS¹⁰ code system. It was found that secondary cosmic-ray neutrons from 10 MeV to several hundreds of MeV was the most significant source of soft errors regardless of the design. This result is of great interest with the FEB in mind as, which is earlier mentioned, circa 80% of the radiation in the FEB is contributed by the DTL with energies up to 90 MeV. The design and geometry of the test device used in [22] is depicted in Figure 4.3.

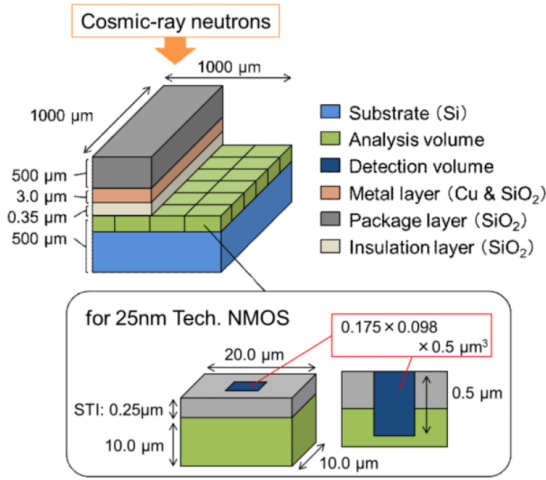


Figure 4.3: Configuration of the test device structure for the 25 nm NMOSFET [22].

Secondary cosmic-ray neutrons cause soft errors as one of the possible consequences of single-event effects. The Soft Error Rates (SERs) were calculated for 25 nm, 32 nm, 45 nm and 65 nm NMOSFETs. During the simulation, neutrons with energies between 1 MeV and 1 GeV were incident on the NMOSFETs. The SERs per bit in an NMOSFET is calculated as

$$SER(Q_c) = \frac{FA}{N_{in}N_{bit}} \int_{Q_c}^{\infty} N(q) dq \quad [22]$$

where Q_c is the critical charge, i.e. the minimum amount of charge needed to flip a data bit, F is the total neutron flux, in $ncm^{-2}s^{-1}$, A is the surface area of the test device, N_{in} is the number of incident neutrons, N_{bit} is the number of bit cells placed in the device and $N(q) dq$ is the number of events in the interval $[q, q + dq]$. The result can be seen in Figure 4.5. Furthermore, it was shown that about 80% of the neutron-induced soft errors were caused by neutrons up to 400 MeV, about 70% were caused by neutrons up to 150 MeV and less than 5% were caused by

⁹PHITS – Particle and Heavy Ion Transport code System

¹⁰HyENEXSS – is a 3D TCAD simulator

neutrons up to 10 MeV, independent of the design rule. This is depicted in Figure 4.4.

Energy group (MeV)	Fraction of neutron flux
1 – 10	0.355
10 – 150	0.441
150 – 400	0.149
400 – 800	0.047
800 – 1000	0.008

Table 4.4: Fraction of incident neutron flux for the studied energy groups in [22].

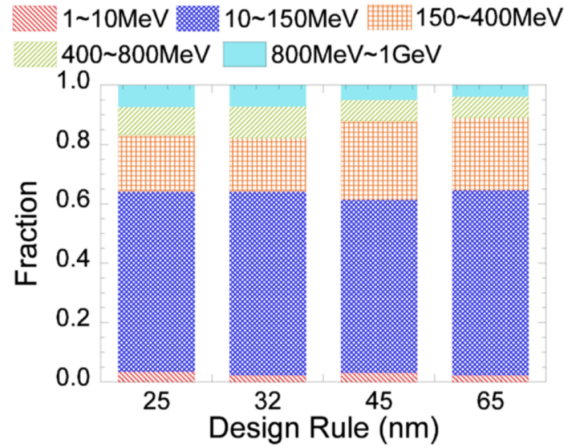


Figure 4.4: The figure presents the soft error contribution of incident-neutron energy range in NMOSFETs of various design rule [22].

The Q_c values used in the calculation yielding the results in Figure 4.5 are 0.6, 0.95, 1.5, and 2.0 fC for NMOSFETs with 25, 32, 45, and 65 nm design rule, respectively.

Furthermore, in [22] it is discussed that the impact of H ions is expected to increase as the critical charge decreases, which is the case as the geometry of a MOSFET is downsized. It is also mentioned that He and H ions may play an essential role as a major cause of neutron induced soft errors.

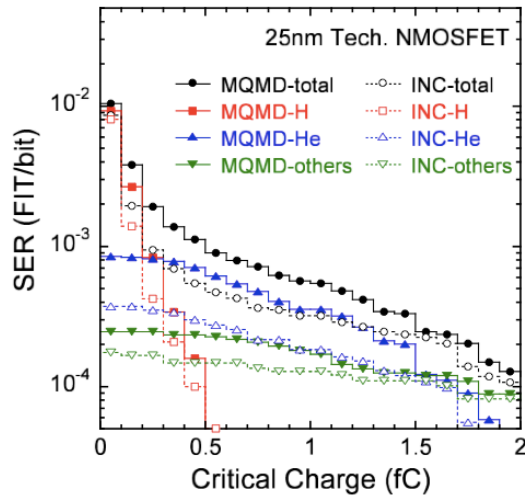


Figure 4.5: SERs per bit calculated with the total neutron flux of $5.94 \cdot 10^{-3} ncm^{-2}s^{-1}$ [22].

4.3.4 Limitations

In this project, it has been found that radiation effects on MOSFETs depend on complex interrelationships such as:

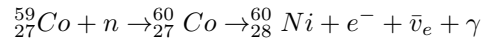
- Energy of the incident particles
- Technology
- Design
- Fabrication procedures
- Conditions of use
- Applied and internal electric fields
- Geometry
- Operating temperature
- Post irradiation conditions
- And more

Furthermore, the difficulty in determining the radiation effects on electronics increases by the fact that microelectronics technologies dramatically change over time. During the past 25 years, MOSFET gate lengths have decreased from $> 10\mu m$ to $< 0.1\mu m$ and the gate dielectric layers from $\sim 70nm$ to $< 2nm$ in commercial technologies. [23] [24]

This poses severe difficulties of designing a simplified generic model for radiation effects on MOSFETs. This matter is further mentioned in Section 7.1.

4.3.5 Radiation hardness calibration

Standard radiation hardness calibration is performed with ^{60}Co as a gamma source. The nuclear equation of the reaction from the stable ^{59}Co isotope to gamma emission is



^{60}Co has desired properties in the sense that it is very well known. Therefore it is often preferred for radiation hardness calibration. For the last 20–25 years, standard test methods for radiation hardness assurance typically use ^{60}Co for gamma source [24]. This potentially causes test result reliability issues as the ^{60}Co gamma emission is mainly of the energies 1.17 MeV and 1.33 MeV. ^{60}Co is artificially produced by adding a neutron to ^{59}Co . The isotope decays to ^{60}Ni and the activated Ni nucleus emits the aforementioned gamma rays.

As discussed in Subsection 4.3.4, the energy of the incident particles play a crucial role in radiation effects on electronics. This is further indicated in [22] and somewhat¹¹ demonstrated in Figure 4.4. This poses the problem that it may be insufficient to calibrate radiation hardness in electronics with a ^{60}Co source. With this in mind, extensive experiments and simulations are hereby suggested necessary.

On December 10, 2014, a presentation was held by Aldo Zenoni, University of Brescia, and Alberto Andrichetto, INFN, at the ESS. The presentation regarded the Radiation Damage Study for SPES on the SPES ISOL-RIB Facility at the INFN Legnaro National Laboratories, Italy. Furthermore, a suggestion of a collaboration with the ESS was expressed. Such a collaboration on radiation damage studies may greatly facilitate the ESS. Furthermore, the potential results from such studies are directly usable in combination with the software tool developed in this project, i.e. STRAM. An experiment guideline proposal is found in Appendix E.

¹¹Figure 4.4 demonstrates the importance of the radiation energies in the sense that different energies contributed to different number of errors as presented in [24]. This may be considered merely as an additive demonstration, and is by no means suggested as an argument.

As mentioned, simulations are used to calculate the radiation in the FEB of the ESS. To understand the nature of these simulations, one must understand the theoretical idea behind them. The Central Limit Theorem is the kingpin of particle simulations and will be discussed along with Monte Carlo Methods, in this chapter.

5.1 Central Limit Theorem

For given independent random variables with defined expected values and variance, the Central Limit Theorem states that the distribution of the frequency of observations will converge towards a normal distribution as the number of observations increase towards infinity.

Theorem 5.2. *(The central limit theorem) Let $\{X_1, \dots, X_n\}$ be i.i.d. random variables with finite expectation μ and finite variance σ^2 , and set $S_n = X_1, \dots, X_n$, $n \geq 1$. Then*

$$\frac{S_n - n\mu}{\sigma\sqrt{n}} \xrightarrow{d} N(0, 1) \quad \text{as } n \rightarrow \infty \quad [25]''$$

The theorem says that the distribution of $\frac{S_n - n\mu}{\sigma\sqrt{n}}$, approximates the normal distribution with mean 0 and variance 1 as n increases.

The advantage of this result is that $\frac{S_n - n\mu}{\sigma\sqrt{n}}$ approaches a normal distribution regardless of the shape of the distribution of the individual X_i . [26]

5.2 Monte Carlo Methods

Monte Carlo Methods are random sampling methods that can be used to approximate the distribution and variance of an unknown probabilistic entity. In some cases this is difficult or even impossible to do analytically or experimentally, and this is when Monte Carlo Methods are very advantageous, e.g. for finding expectation values of quantum mechanical operators. [27]

As the Central Limit Theorem shows that $\frac{S_n - n\mu}{\sigma\sqrt{n}}$ approaches a normal distribution regardless of the shape of the distribution of the individual X_i , Monte

Carlo can be used to find the standardized normal distribution $N(0, 1)$ for any system.

5.3 Monte Carlo radiation transport codes

Investigating radiation effects is a complex issue. The assessment requires detailed descriptions of the relevant energy spectra and radiation quantities.

5.3.1 FLUKA

Fluktuierende Kaskade (FLUKA) is a multi-purpose particle interaction and transport code. This tool is used for calculating proton-proton and heavy ion collisions in a wide range of energies. With high accuracy, FLUKA can be used to describe the hadronic and electromagnetic particle cascade initiated by secondary particles. It is an integral code of all radiation damage studies to electronics. It has been used extensively in experimental areas as well as for studying electronics failures at intensive beam loss regions around the Large Hadron Collider (LHC) accelerator. In [28], it is discussed that LHC alcoves equipped with commercial electronics are affected the most by SEEs, which is further discussed in Section 4.3. Electronics installed in the LHC tunnel, however, suffers from accumulated damage, which is also discussed in Section 4.3. [28]

5.3.2 Monte Carlo N-Particle Transport Codes

Monte Carlo N-Particle (MCNP) transport codes, are codes that can be used for neutron transport. The code is well suited for radiation protection and dosimetry, radiation shielding, radiography and accelerator target design among other areas.

Pointwise cross section data as well as group-wise data can be used. For neutrons, reactions given in a particular cross section evaluation are accounted for. MCNP possesses powerful features, which include computation with respect to energy, intensity, direction, shape, temporal characteristics, volume, coordinates and more. This is, in fact, the codes used for generating the radiation maps necessary for the software development in this project.

Software Development

Software Tool for Radiation Absorption Maps (STRAM), is a tool developed with the purpose of reading maps of particle fluxes and energy spectra, then folding the information with response functions of electrical equipment and materials. The tool produces a map, revealing the expected absorbed dose at each position for which the original radiation map was produced. In other words, by providing the tool with a radiation map of a room and the response of a device, the tool will generate a radiation energy absorption map for the given device in that particular room. Consequently, this can be used to find the optimal location of a device, should it be feasible to be chosen arbitrarily. Should this not be the case, necessary shielding measures or conclusions regarding other options, may be derived from the results. The capabilities of STRAM for prediction of radiation damage to electronics has been presented. STRAM demonstrates applicability in all radiatory environments, provided a radiation map is generated.

The result of this software opens up to a global collaboration by enabling every research facility to contribute to a library of electronics response functions. For this to be feasible, however, a data base must be designed. Such a database lies outside this thesis.

6.1 ROOT

For the development of STRAM, the ROOT system and C++ programming language has been used. ROOT is a system with a built-in CINT C++ interpreter with a set of object-oriented frameworks, developed by the Physics Department at CERN. The system is advantageous for handling and analysing large amounts of data efficiently.

In this project, computationally efficient histogram methods in several dimensions have been used to represent the information contained in the absorption maps of STRAM, which will be explained further in Section 6.2. Graphics and visualization classes of ROOT is then used to visualize the results.

6.2 STRAM

6.2.1 Radiation map

For radiation mapping, MCNP has been used to calculate the gamma and neutron radiation in the FEB of the ESS. The radiation has been characterized in terms of quantities and energy spectra. The information from the MCNP simulations is stored in histograms within a ROOT-file. The ROOT-file is imported by STRAM, which extracts the information from the histograms to create a new histogram of four dimensions. Three dimensions represent Cartesian coordinates in space whereas the fourth dimension represents the energy spectra of the flux in a given geometrical position.

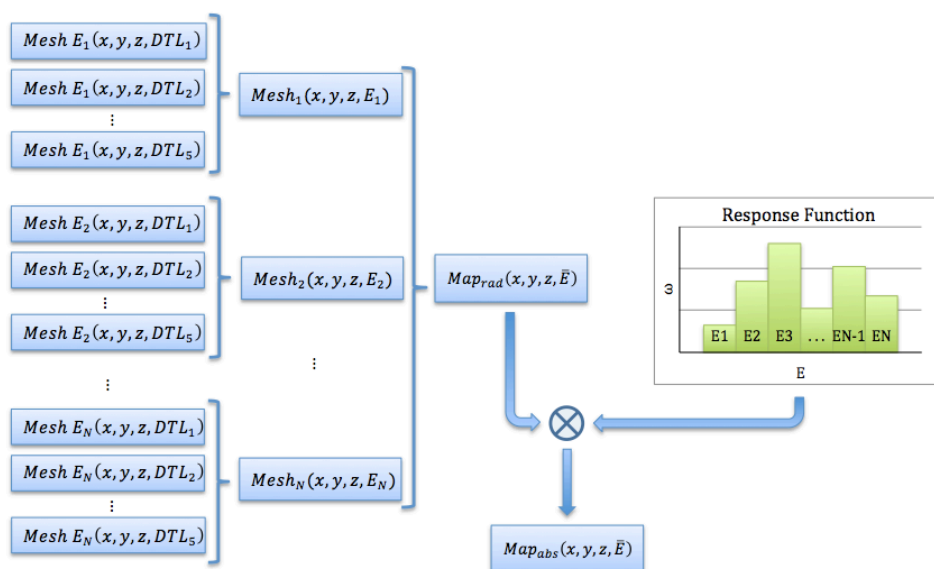


Figure 6.1: The chart illustrates the idea behind the computation of the absorption map.

In Figure 6.1 the radiation contribution from the DTL tanks 1 through 5 in the accelerator tunnel, to the FEB of the ESS, are simulated and mapped for different energies. Maps have been generated for each DTL tank and various energies. The maps for all tanks of certain energy is shrunk down to one map, specific for one energy. Finally, the maps for all energies contribute to a full desired energy spectrum into one radiation map, called Map_{rad} in the figure. The Map_{rad} contains information of location in Cartesian coordinates as well as the flux and energy spectra at each point. Folding the Map_{rad} and the response function for a given device, yields the absorption map Map_{abs} . Note that the number of energy intervals, N , for which the radiation map has been generated, matches the number of bins in the response function. This is necessary for the folding to be feasible.

In Figure 6.2, an example of a radiation map in STRAM is illustrated. The preliminary schematics of the FEB as seen in Figure 3.2, is illustrated with hypo-

thetical radiation maps in Figure 6.3. This provides an intuitive idea of what the radiation map resembles inside the FEB.

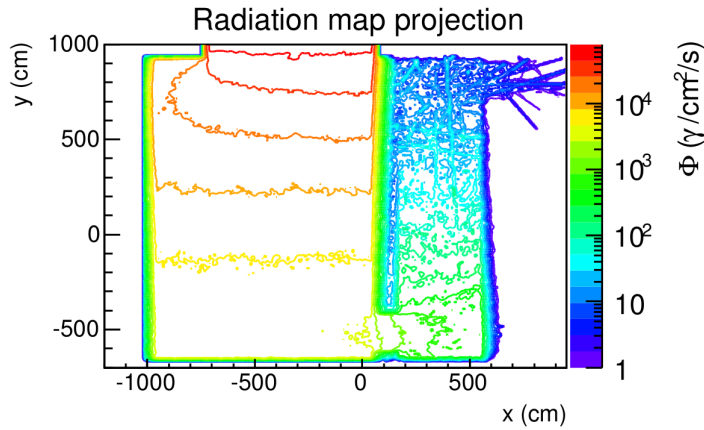


Figure 6.2: The figure presents an example of a radiation map. The origin of the $x-y$ system is an arbitrarily chosen reference point in the FEB. For an intuitive idea of how this radiation map could look in the FEB, see Figure 6.3.

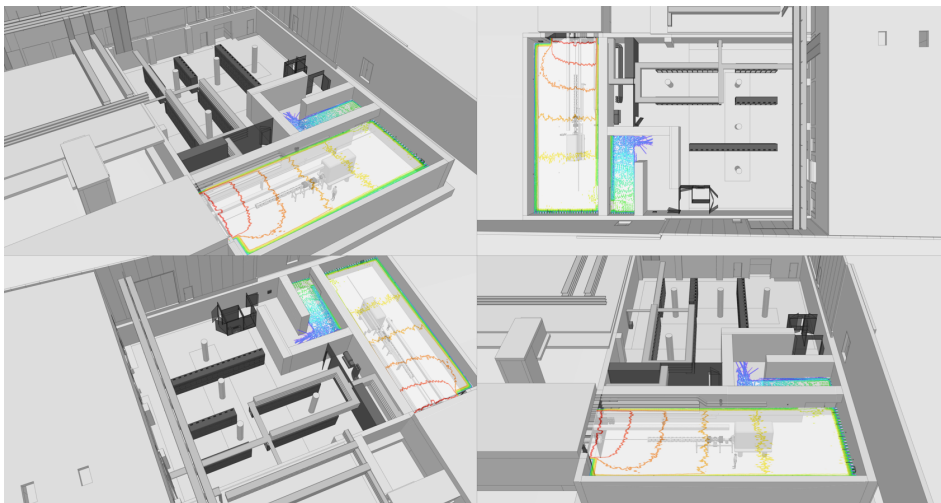


Figure 6.3: An illustration of a hypothetical radiation map inside the FEB of the ESS.

6.2.2 Response function

The response function for an electronic device or a material in a radioactive environment is very complex. This depends much on the fact that the absorbed dose is correlated to the cross section. As discussed in Section 2.1.3, cross sections describe the probability of a given nuclear reaction to occur. As this depends on many attributes of the interacting particles, the cross section, and thus the response function, becomes very complex. Furthermore, the fact that a device is not a single element but a construction of various components, some of which in turn are constructed of various materials and alloys, complicates the response function further.

Response functions can be generated through simulations and experiments. The response function to be produced is merely an expression of probability of the radiation energy absorption. However, with sufficient data, this may be sufficiently accurate to generate reliable results.

Response functions for nitrogen, obtained by means of simulation, has been provided by Research Associate, Eduardo Nebot del Busto, CERN. The nitrogen is used as filling of the Beam Loss Monitoring detectors and response functions have been produced for various particles and various incident angles. From this information, a response function has been designed to reveal the absorbed dose in terms of Gy/h, caused by gamma radiation¹². The new response function considers all incident angles of the gammas. The original information is presented in histograms as seen in Figure C.1 and C.3 in Appendix C. To be able to fold this information with the radiation map, the binning is reduced to match the binning of the radiation map. Consequently, the resolution of the energy spectra are determined by the component of lower resolution. The resolution of the results is therefore decided when the radiation maps and response functions are generated.

The binning of the histograms is reduced to represent the same energy spectra as the radiation map, with one bin per energy interval. The radiation map in this report has been chosen to represent a spectrum from 100 keV-100 MeV in order to cover the energies present in the FEB. The resulting response function for this thesis is seen in Figure 6.4.

6.2.3 Absorption map

A class *AbsorptionMap* has been developed for the software. An *AbsorptionMap* object is initially constructed from an input vector of file names. The file names are used by STRAM to import the files that contain the radiation information from the room for which the absorption map is desired to be defined. Recall that the radiation information is obtained through Monte Carlo Simulations as discussed in Chapter 5. When the object is created, it gathers all information from the files of the input file names and generates a single map for the radiation. An arbitrary response function from a separate ROOT-file can then be set to the object. When the response function is set, the software immediately generates a map with the

¹²The calculations to redefine the response function in order to reveal the absorbed dose in Gy/h is described in Appendix C

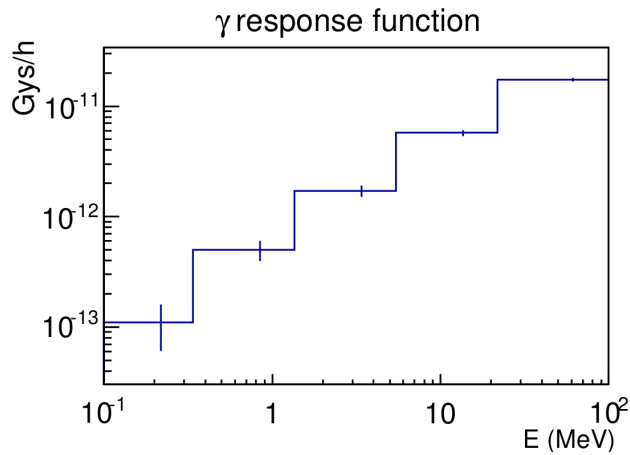


Figure 6.4: Nitrogen response function for γ -radiation

folding of the radiation map and the response function. The resulting map is the aforementioned absorption map.

If a response function has been set to the radiation map, the class draw function `AbsorptionMap::Draw(Option_t *option)` automatically draws radiation map, response function and absorption map. Should the response function not be set, the draw function will only draw the radiation map. In Figure 6.5, the initial interface of a drawn `AbsorptionMap` is shown. In the top left figure, a three-dimensional representation of the radiation is presented. In the top right figure, a two-dimensional logarithmic representation of the radiation map is found. The bottom left figure shows the response function of a selected device and the bottom right figure shows the resulting absorption map.

As for the error propagation in the computation of histogram content, ROOT includes recalculation of errors when executing histogram content operations. The concept of error propagations has been moderately studied but will not be further discussed in this report. However, some of the ideas behind the error propagation used, can be found in [29].

6.2.4 GUI

The interactive aspect of the design enables energy spectra analysis. When the mouse is hovered in the *Radiation map projection* seen in Figure 6.6, the energy spectra at that location will be displayed in *Radiation energy spectra of binX=x, binY=y*, where x and y are the coordinates for the position of the mouse. It is possible to prevent auto update of the spectra by simply clicking with the mouse at the location where a desired spectra is found. By clicking in the *Absorption map projection*, auto update is reinstated and the spectra for an arbitrary location in the *Absorption map projection* can be studied. This function may be interesting as it opens up to the possibility of comparing the energy spectra of the original radiation and the spectra of the absorbed dose.

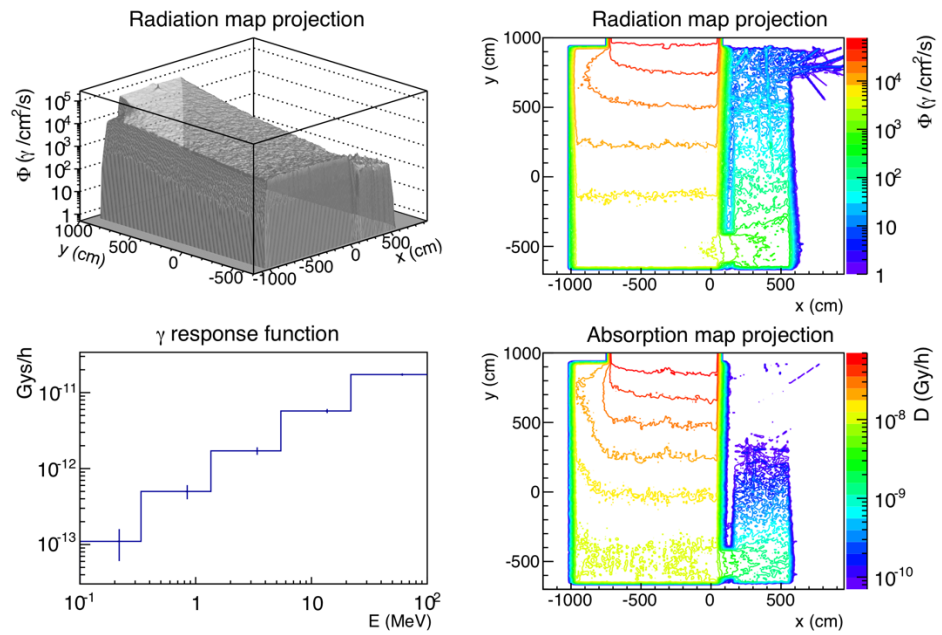


Figure 6.5: STRAM initial interface.

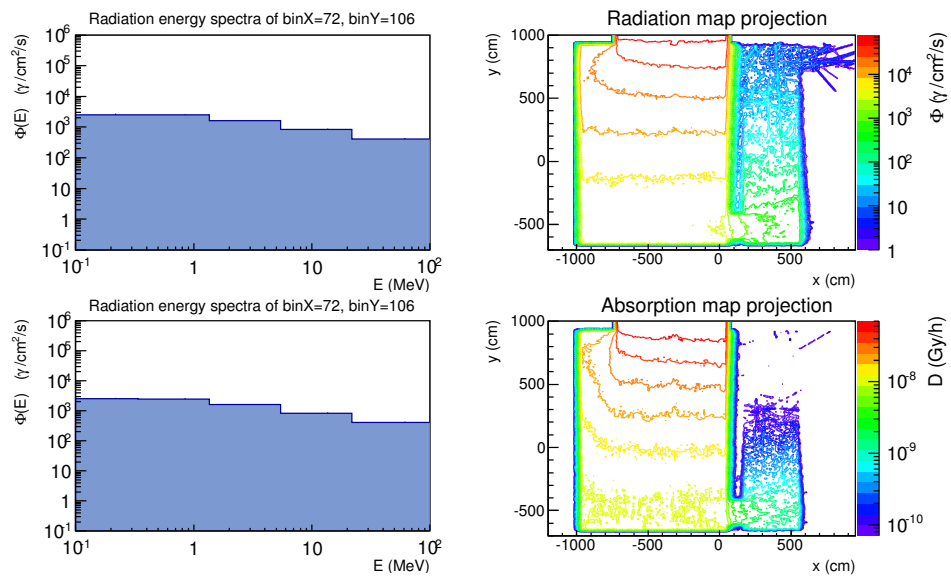


Figure 6.6: STRAM interface during interaction.

Evaluation and conclusion

The approach throughout this thesis is based on determining desired results and various goals, to then deeply immerse into the theory behind the problems, whilst leaving behind a strand of yarn. This way, a link between the basic theory and the end product and ideas, is always clear. By considering radiation effects on electronics it was decided to focus on MOSFET, given its importance in electrical circuits. In order to understand the MOSFET one must understand the BJT and p-n junction. In other words, by descending from a problem and dig to the very core of it. The approach has been proven fruitful in this project and on top of a better understanding of radiation effects on electronics, a software tool has been developed to aid in the assessment of such effects. An evaluation and conclusion of this work is presented in this chapter.

7.1 Radiation effects on electronics

Radiation effects on electronics can be divided into two main categories, cumulative effects and SEEs. Particular interest has been paid to cumulative effects, foremost TID. This choice is made due to the importance of TID in this project, as it connects much to the MOSFET which is found in all digital circuits. Issues that may occur due to TID include threshold voltage shifts, device degradation due to charge build-up in the SiO_2 gate insulator, and increased power consumption due to leakage of trapped charges. The leakage is a quantum phenomenon where the charges escape by means of tunnelling effects. Mainly gammas and neutrons have been considered for the radiation effects on electronics, however gammas are used for simulation examples with STRAM throughout this report.

This thesis mentions many limitations in regard to analytically predict radiation effects on electronics. Therefore, a simplified model for accurate predictions of TID effects is not available and, thus, extensive simulations and experiments may be preferred. As a simplified model is unavailable, it may be interesting to research the possibility of designing algorithms for a radiation weighting factor for electronics, similar to the weighting factor for human tissue presented in Section 4.2. This suggestion for future work is further discussed in Section 7.3.

The aforementioned limitations refer to the fact that the effects of TID on MOSFETs and integrated circuits are very complex. They depend on a large number of parameters among which we find: Fluence, incident particle energy,

applied and internal electric fields, technology, geometry, material, fabrication process (e.g. the process of oxide growth), oxide impurities, operating temperature, and conditions of use, and more [23].

An important discussion in Subsection 4.3.5, addresses the issues of ^{60}Co calibration for radiation hardness of electrical devices. The ^{60}Co gamma emission is mainly of the energies 1.17MeV and 1.33MeV. As discussed in Subsection 4.3.4, the energy of the incident particles play a crucial role in radiation effects on electronics. This is further indicated in [22] and further demonstrated in Figure 4.4.

To find an adequately accurate response function, it is hereby suggested to simulate charge build-up such as presented in [21]. For application at the ESS, such simulations must be performed in the relevant energy intervals. The radiation maps for the area at which a given device is desired to be located must then, as earlier discussed, be defined for the same energy intervals.

The assessment of radiation effects on electronics is complex. The research of these effects reaches beyond this thesis, however this report provides a certain insight in the matter as well as a useful software tool to aid.

7.2 STRAM

For very rough initial radiation analyses, it may be desired to use point simulations for obtaining radiation flux at a given location. For a more detailed description of an area, however, STRAM demonstrates applicability in all areas where significant radiation is present e.g. particle accelerators, nuclear power plants, space and hospitals. STRAM can be used to make approximate predictions and studies of radiation effects on any material, i.e. it can be used for any element, polymer, human tissue, alloy or entire device. As a disclaimer, it must be mentioned that the software may not be sufficiently tested to guarantee that error propagations and histogram contents are flawlessly computed, and hence, further development is advised.

The tool allow visualization of Monte Carlo simulated radiation maps. If a response function is supplied to the tool, the tool folds the radiation map with the response function and reveals the amount of absorbed dose. Furthermore, the tool is interactive. As not only the flux is interesting, but also the energy spectra, the spectra can be seen for each location in the radiation- and absorption map by simply hovering the mouse in a map. An auto update of the energy spectra can be activated and deactivated by clicking with the mouse inside a map. This offers the possibility of studying the energy spectra as well as compare the energies of the radiation in a room with the absorbed dose.

7.3 Improvements and future work

7.3.1 Radiation weighting factors for electronics

As a simplified model is unavailable, it may be interesting to research the possibility of designing algorithms for a radiation weighting factor for electronics, similar to

the weighting factor for human tissue presented in Section 4.2. There may be a possibility that a response function for one particle type could be sufficient and that radiation weighting factors could translate the radiation effects between various incident particles. If so, it would save an immense amount of time, effort and finances. Therefore, future research in this matter is hereby recommended.

7.3.2 Chebyshev nodes

For future development of automatic binning of response functions, an idea for response function resolution is to exploit Chebyshev nodes. In numerical analysis, Chebyshev nodes are commonly used as roots for the interpolating Chebyshev polynomial which minimizes the effect of Runge's phenomenon [30] [31]. For the purpose of generating accurate response functions, however, Chebyshev nodes may be preferable due to their distribution. Chebyshev nodes are distributed in such a way that errors are more evenly distributed, and the maximum error is minimized. If the nodes are chosen over a desired interval of energies, with respect to the curve of the cross section for a given reaction, the binning of the response function can be improved.

For nodes over an arbitrary interval $[a, b]$

$$x_k = \frac{1}{2}(a + b) + \frac{1}{2}(b - a) \cos\left(\frac{2k - 1}{2n}\pi\right), k = 1, \dots, n. \quad [30] \quad (7.1)$$

and the binning of the response function should be centered around each node [30]. Note, however, that the radiation map energy spectra must have the same binning as the response function for the approach of Chebyshev nodes to be of value.

A certain, and crucial, trade-off is to be considered. Binning the response function based on Chebyshev nodes will minimize the ∞ -norm, i.e. the maximum error. However it leaves no room for arbitrarily choosing the bin width, meaning that the energy interval of each bin will be decided by the Chebyshev nodes. This will give a representation closer to the measurements that provided the original data for the response function, but prevents possibly desired energy intervals of the bins. This is of importance as specific intervals may have higher probability of certain radiation effects on the device in question, hence, it may be preferable to choose the binning based on the possible radiation effects rather than a more accurate representation of the measurements. An example of the benefits of Chebyshev interpolation with Chebyshev nodes is presented in Appendix B.

7.3.3 Location optimization in STRAM

Given the strategy of relocation of a device to minimize radiation damage, one may search for a location with acceptable flux and energy spectra by observing the absorption map provided by STRAM. For efficiency however, it may be desired to implement optimization algorithms to find a location, given constraints on flux and/or energy spectra. It may be relevant to consider a trade-off between which energies to avoid and the magnitude of the flux to be allowed.

Furthermore, it should be suggested that a more complex algorithm is designed, taking several constraints into account. The idea is to enable the user

to define hard and soft constraints, e.g. cable length to the device, flux, energy spectra, distance from some given point etc. Given that a feasible solution exists, the algorithm should find a solution that does not violate the hard constraints, whilst minimizing the violation of the soft constraints.

7.3.4 Shielding investigation in STRAM

The algorithm suggested in Subsection 7.3.3 may be used a priori shielding considerations, should it be feasible to choose location. Furthermore, the algorithm may be improved to account for shielding, i.e. location is chosen by the algorithm such that violation of constraints are countered by shielding which is calculated to its minimum whilst guaranteeing sufficient protection with a desired confidence interval.

7.3.5 Web based version of STRAM

With the current version of STRAM, the user must have ROOT installed on their computer for the code to run. With a web based tool, however, only the server which will run the code must have the proper systems installed. Such a web page may also include the aforementioned data base of response functions.

Bibliography

- [1] United States Department of Energy Fermilab, Office of Science. The standard model of elementary particles the 12 fundamental fermions and 4 fundamental bosons, currently known by science.
- [2] Paul A. Tipler and Gene Mosca. *Physics For Scientist and Engineers*. W. H. Freeman and Company New York, sixth edition, 2008.
- [3] William S. Rodney Claus E. Rolfs. *Cauldrons in the Comsos; Nuclear Astrophysics*. Theoretical Astrophysics series. The University of Chicago Press, 1988.
- [4] Anders Gustafsson. *Komponentfysik - En introduktion*. Lund University, Faculty of Engineering, LTH, 7th edition, 2011.
- [5] B. E. A. Saleh and M. C. Teich. *Fundamentals of Photonics*. John Wiley & Sons, 1991.
- [6] ESS European Spallation Source. <http://europeanspallationsource.se>.
- [7] Steve Peggs, editor. *Technical Design Report*. The European Spallation Source, April 2013.
- [8] Accelerator integration master model ess-0016885.
- [9] Accelerator decision – conventional facilities coordination input file ess-0012419.
- [10] *Compendium of Dose Coefficients based on ICRP Publication 60*, number 119. Elsevier, pages 9-11, 2012.
- [11] Swedish Radiation Safety Authority. *Swedish Radiation Safety Authority Regulatory Code*, volume 51, 2008.
- [12] Swedish Radiation Safety Authority. *Special Conditions for the ESS Facility in Lund*, number 13-3285, June 2014.
- [13] *Compendium of Dose Coefficients based on ICRP Publication 60*, number 119. Elsevier, 2012.
- [14] Mohsen Razavy. *Quantum Theory of Tunneling*. World Scientific, 2003.

-
- [15] Andre Kessler. Derivation of the heisenberg uncertainty principle. url: <http://www.tjhsst.edu/2011akessler/notes/hup.pdf>.
- [16] Marc Poizat. Total ionizing dose mechanisms and effects. eesa - EPFL Space Center, June 2009.
- [17] Ken Wyllie. Radiation hardness assurance. Technical report, European Space Components Information Exchange System, ESCIES, 2014.
- [18] Luisella Lari. *Beam-Machine Interaction Studies for the Phase II LHC Collimation System*. PhD thesis, École Polytechnique Fédérale de Lausannes, 2010.
- [19] Jean-Marie Lauenstein. *Single-event Gate Rupture in Power MOSFETs: A New Radiation Hardness Assurance Approach*. PhD thesis, University of Maryland, 2011.
- [20] R. Koga et al. Single event functional interrupt (sefi) sensitivity in microcircuits. *IEEE Xplore*, 1997.
- [21] H. E. Boesch et al. Saturation of threshold voltage shift in mosfets at high total dose. *IEEE Transactions on Nuclear Science*, NS-33(6), December 1986.
- [22] S. Abe Y. Watanabe. Nuclear reaction models responsible for simulation of neutron-induced soft errors in microelectronics. *ScienceDirect*, pages 254–257, July 2014.
- [23] H. L. Hughes and J. M. Benedetto. Radiation effects and hardening of mos technology: Devices and circuits. *IEEE Transactions on Nuclear Science*, 50(3):500–521, 2003.
- [24] D. M. Fleetwood and H. A. Eisen. Total-dose radiation hardness assurance. *IEEE Transactions on Nuclear Science*, 50(3):552–564, 2003.
- [25] Allan Gut. *An Intermediate Course in Probability*. Springer, second edition, 2009.
- [26] Patrick Billingsley. *Probability and Measure*. John Wiley & Sons, third edition, 1995.
- [27] Morten Hjorth-Jensen. *Computational physics*. University of Oslo, 2010.
- [28] Giuseppe Battistoni et al. FLUKA capabilities and CERN applications for the study of radiation damage to electronics at high-energy hadron accelerators. *Progress in Nuclear Science and Technology*, 2:948–954, 2011.
- [29] John R. Taylor. *An Introduction to Error Analysis*. University Science Books, second edition, 1997.
- [30] J. Douglas Faires Richard L. Burden. *Numerical Analysis*. Thomson Brooks/Cole, 8th edition, 2005.
- [31] G. W. Stewart. *Afternotes on Numerical Analysis*. Siam, 1996.
- [32] Evaluated Nuclear Data File (ENDF). Database version of october 22, 2014. <https://www-nds.iaea.org/exfor/endl.htm>.

ESS

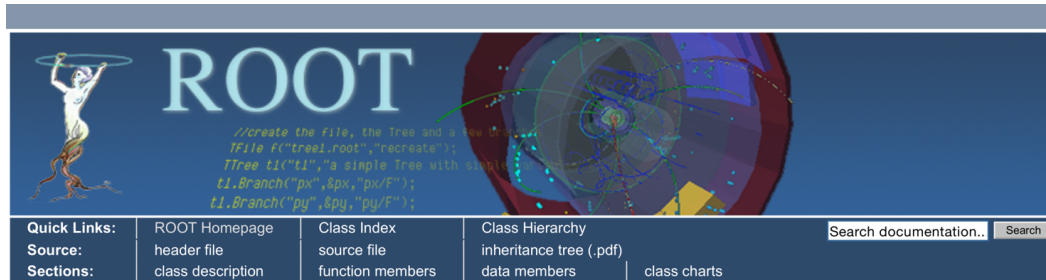
TARGET DIVISION

Johannes C. Kazantzidis

johannes.kazantzidis@esss.se

Software Documentation

The software code documentation is presented as a generated .html, following the conventions of ROOT and C++. However, with the source code for the scripts generating the code documentation, a user may type *make doc* in the terminal to generate the documentation in .html format. The generated file will then contain links to the source code of all methods.



The ROOT logo features a figure holding a ring, with the word "ROOT" in large letters. Below it is a snippet of C++ code:


```
//create the file, the Tree and a file
TFile f("tree1.root","recreate");
TTree t1("t1","a simple Tree with some data");
t1.Branch("px","&px","px/F");
t1.Branch("py","&py","py/F");
```

 To the right is a 3D visualization of a particle detector. Below the logo is a navigation menu with the following items:

- Quick Links: ROOT Homepage, Class Index, Class Hierarchy
- Source: header file, source file, inheritance tree (.pdf)
- Sections: class description, function members, data members, class charts

 A search bar is located on the right side of the menu.

Absorption map » SRC » AbsorptionMap

class AbsorptionMap

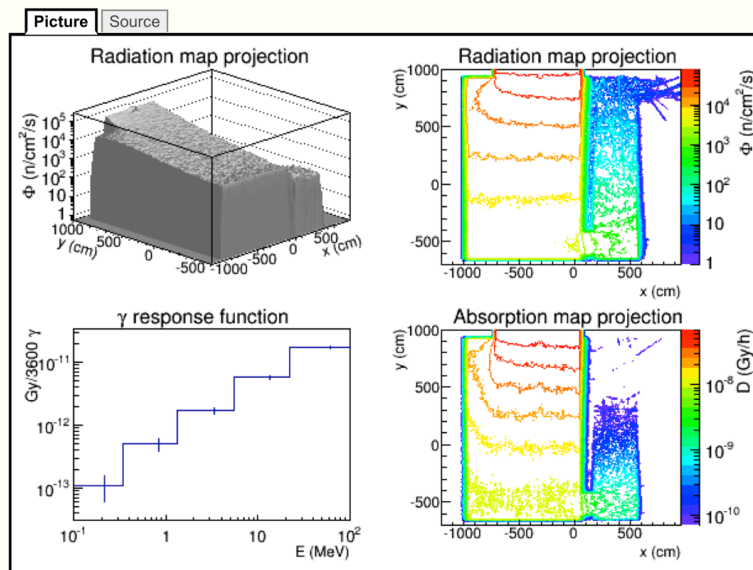


AbsorptionMap class

An *AbsorptionMap* is an object which reads ROOT files containing sparse histograms with radiation mesh tallies and generates a radiation map. Such ROOT files can be generated by first performing Monte Carlo simulations to obtain radiation mesh grids and secondly, using *mtal2root* to convert the Monte Carlo simulations to *.root* format.

By setting a response function to the object, *AbsorptionMap* folds the radiation map with the response function and generates a map revealing the absorbed dose of the object which the response function represents.

The picture below gives an example:



Introduce response function

Introducing a response function to an *AbsorptionMap* object, enables the computation and drawing of a map revealing the absorbed dose. Setting a response function is performed as follows:

```
AbsorptionMap *a1 = new AbsorptionMap("a1 title", TString vector of filenames);
a1->SetResponseFunction("file name");
```

Introduce reponse function

Introducing a response function to an AbsorptionMap object, enables the computation and drawing of a map revealing the absorbed dose. Setting a response function is performed as follows:

```
AbsorptionMap *a1 = new AbsorptionMap("a1 title", TString vector of filenames);
a1->SetResponseFunction("file name");
```

Draw a map revealing the absorbed radiation

Drawing a absorption maps requires a TCanvas as well as a response function (see Introduce reponse function). Drawing the maps is hence performed as follows:

```
AbsorptionMap *a1 = new AbsorptionMap("a1 title", TString vector of filenames);
a1->SetResponseFunction("file name");
TCanvas *c1 = new TCanvas();
a1->Draw();
```

Acknowledgements

Recognition goes to Nicolo Borghi and Konstantin Batkov for the development of mctal2root, without which this class could not have been created. Special thanks goes to Riccardo Bevilacqua for his ideas to this class, and to Konstantin Batkov for invaluable help with programming.

mctal2root

With the mctal2root converter, ASCII MCTAL files produced by MCNPX are converted into binary ROOT files containing a set of [THnSparseF], one for each tally. More about mctal2root can be found at [here](#).

Function Members (Methods)**public:**

```

    AbsorptionMap (const AbsorptionMap&)
    AbsorptionMap (const char*, vector<TString>)
    virtual ~AbsorptionMap ()
    static void AbsExec (THnSparseF* hist, TPad* pad, Int_t, Int_t, Int_t, TH1F* rfhist = 0)
    static TClass* Class ()
    virtual void Draw (Option_t* option = "")
    virtual TClass* IsA () const
    void SetResponseFunction (const char*)
    virtual void ShowMembers (TMemberInspector&)
    virtual void Streamer (TBuffer&)
    void StreamerNVirtual (TBuffer& ClassDef_StreamerNVirtual_b)
```

private:

```

    void CreateMesh (TString)
    void GenerateAbsMap ()
    void GenerateRadMap ()
    Double_t GetAbsContent (Int_t, Double_t)
    void GetMeshGrids ()
```

Data Members

private: THnSparseF* fAbsMap Int_t fAbsMax const char* fAbsName static Bool_t fAutoUpdate vector<TString> fFileNames Bool_t fIsAbsMap Int_t fMeshCount const char* fName Int_t fNumberOfFiles TH1F* fRF Int_t fRFBins TString fRFName THnSparseF* fRadMap Int_t fRadMax const char* fRadName vector<THnSparseF*> fRmesh Int_t fX Int_t fY Int_t fZ	-> Pointer to absorption map Maximum value of bin content in absorption map -> Pointer to absorption map name Flag to enable/disable auto update of energy spectra for maps Names of imported files Flag to generate absorption map Number of imported mesh grids -> Pointer to object name Number of imported files -> Pointer to response function histogram Number of bins in response function histogram Response function file name -> Pointer to radiation map. Maximum value of bin content in radiation map -> Pointer to radiation map name Imported mesh grids Number of bins x dimension of radiation map Number of bins y dimension of radiation map Number of bins z dimension of radiation map
---	--

Class Charts

Inheritance Chart:

AbsorptionMap

Function documentation

AbsorptionMap (const char* , vector<TString>)

Constructor

~AbsorptionMap ()

Destructor

void **GetMeshGrids** ()

Extract mesh grids from imported files. Acceptable mesh grids have 11 dimensions and will be added to the private class member vector `fRmesh`.

void **CreateMesh** (TString)

Create a sparse histogram for radiation map with correct attributes.

void GenerateRadMap ()

Extract information from all mesh grids in `fRmesh` to generate the radiation map `fRadMap`.

void SetResponseFunction (const char*)

Set response function for a given device or material. A map revealing the radiation absorption of the device, in the room for which the radiation map has been produced, will be generated.

Double_t GetAbsContent (Int_t, Double_t)

Fold radiation with response function at a given location in the room for which the radiation map has been produced.

void GenerateAbsMap ()

Extract information from radiation map and response function to generate the absorption map `fAbsMap`.

void AbsExec (THnSparseF* hist, TPad* pad, Int_t, Int_t, Int_t, TH1F* rhist = 0)

`AbsExec` listens to mouse events for interaction with a radiation map and/or the absorption map. Hovering mouse over a map will generate energy spectra histogram, a left mouse click inside a map will lock the energy spectra histogram.

void Draw (Option_t* option = "")

Draw interactive maps.

AbsorptionMap (const char*, vector<TString>)

Constructor

Chebyshev Interpolation Example

Consider the function

$$f(x) = \frac{e^x}{1 + 25x^2}$$

Consider the polynomial fitting $p(x) = f(x_i)$, where x_i is an interpolation node.

The Chebyshev nodes serve to minimize the ∞ - *norm* of the error, i.e. minimizing

$$\max_{x \in [-1, 1]} \left| \prod_{i=1}^n (x - x_{Chebyshev_i}) \right|$$

Let $\bar{x}_{equidistant}$ be 10 equidistant nodes in the interval $[-1, 1]$ and let $\bar{x}_{Chebyshev}$ be Chebyshev nodes on the same interval, defined as

$$\cos\left(\frac{2k-1}{2n}\pi\right), k = 1, 2, \dots, n$$

where $n = 10$. Let $p(x)$ be a polynomial of order 9. For the given function $f(x)$, the errors are computed to be

$$\epsilon_{equidistant} = 0.5641$$

$$\epsilon_{Chebyshev} = 0.2645$$

The following MATLAB code presents the discussed calculations and a plot of the result is seen in Figure B.1.

```
f = @(x) exp(x)./(1+25.*x.^2);
x = linspace(-1,1);

x_equidistant = linspace(-1,1,10);
p = polyfit(x_equidistant, f(x_equidistant), 9);
plot(x, polyval(p,x), 'r');hold on;grid on;
plot(x, f(x))
error_equidistant = max(abs(f(x)-polyval(p,x)))

k = 1:10;
```

```

n = max(k);
x_Chebyshev = cos((2*k-1)*pi/(2*n));
q = polyfit(x_Chebyshev, f(x_Chebyshev), 9);
plot(x, polyval(q,x), 'g')
legend('f(x) = exp(x)/(1+25*x^2);', 'Equidistant ...
      Chebychev Interpolation', 'location', ...
      'NorthWest')
xlabel('x')
ylabel('y')
error_Chebyshev = max(abs(f(x)-polyval(q,x)))

```

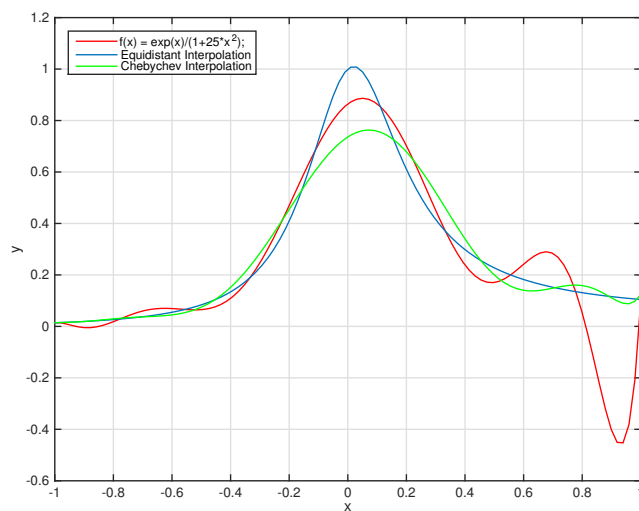


Figure B.1: The figure illustrates the interpolation with equidistant nodes and Chebyshev nodes for the function $f(x) = \frac{e^x}{1+25x^2}$

CERN Data

For illustrative purposes, data obtained from CERN in ROOT-format is treated and presented in this appendix. Following code is written in ROOT, presenting the data along with two of the histograms.

```
root [0] TFile *f = TFile::Open("new_resp_200908.root")
root [1] f->ls()
TFile**      new_resp_200908.root
TFile*       new_resp_200908.root
KEY: TDirectoryFile  00deg;1 00deg
KEY: TDirectoryFile  15deg;1 15deg
KEY: TDirectoryFile  30deg;1 30deg
KEY: TDirectoryFile  45deg;1 45deg
KEY: TDirectoryFile  60deg;1 60deg
KEY: TDirectoryFile  75deg;1 75deg
KEY: TDirectoryFile  85deg;1 85deg
KEY: TDirectoryFile  90deg;1 90deg
root [2] TDirectoryFile *df = f->Get("00deg")
root [3] df->ls()
TDirectoryFile*      00deg  00deg
KEY: TH1D  rf_mu_p;1  mu+ at 0deg
KEY: TH1D  rf_mu_m;1  mu- at 0deg
KEY: TH1D  rf_e_m;1   e- at 0deg
KEY: TH1D  rf_e_p;1   e+ at 0deg
KEY: TH1D  rf_kaon_m;1 kaon- at 0deg
KEY: TH1D  rf_kaon_p;1 kaon+ at 0deg
KEY: TH1D  rf_pi_m;1  pi- at 0deg
KEY: TH1D  rf_pi_p;1  pi+ at 0deg
KEY: TH1D  rf_proton;1 proton at 0deg
KEY: TH1D  rf_gamma;1 gamma at 0deg
KEY: TH1D  rf_neutron;1 neutron at 0deg
KEY: TH1D  rf_neutron150;1 neutron 150 bins at 0 deg
root [4] TH1 *h = df->Get("rf_gamma")
root [5] h->Scale(34.8)
root [6] h->SetXTitle("E_{k} (eV)")
root [7] h->SetYTitle("E_{dep} (eV)")
root [8] gStyle->SetOptStat(0);
root [9] h->Draw()
```



```

Info in <TCanvas::MakeDefCanvas>: created default TCanvas ...
      with name c1
root [10] c1->SetLogx()
root [11] c1->SetLogy()
root [12] h->GetXaxis()->SetTitleOffset(1.3);

```

Figure C.1 presents a response function in the form of a histogram. The figure shows the nitrogen response function for neutrons of 0° incident angle. 0° incident angle implies that the particle enters on axis of the ionization chamber used in the simulation and 90° implies that the incident particle is perpendicular to the chamber axis. The data is presented in a histogram of 150 bins. The x-axis represents the kinetic energy of the particle. The y-axis represents the charge detected by the chamber multiplied with a weighting factor ω for the average energy necessary to produce an electron ion pair in nitrogen, which is $\omega = 34.8eV$. This charge detected by the chamber is derived as $q = \frac{E_{dep}}{\omega}$, where E_{dep} is the deposited energy and ω is the weighting factor.

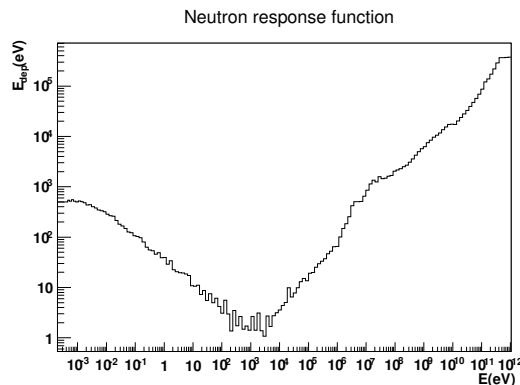


Figure C.1: The figure presents data from CERN, illustrating the nitrogen response function for neutrons.

Note that for lower energies of the incident neutron, more energy is deposited than that of the neutron. This is possible because the nitrogen that absorbs a neutron may become an unstable oxygen isotope, which then decays and emits γ and β of much higher energy than that of the incident neutron. This phenomena is also discussed in Subsection 2.1.2.

Furthermore, note the fluctuations in the neutron response function, particularly in the interval ($1eV - 10^5eV$). At first sight, one may come to think of cross section fluctuations, however the data fluctuations has been found to not necessarily be correlated to the neutron-nitrogen cross section. In Figure C.2, the nitrogen response function data from CERN is compared with the neutron cross section. The cross section fluctuations are seen in circa ($5 \cdot 10^5eV - 50 \cdot 10^7eV$), which evidently is different from the interval of fluctuation in the response function. It is therefore concluded that the fluctuations do not come from the cross section. Instead, a reasonable idea is that this possibly depends on binning or simulation properties.

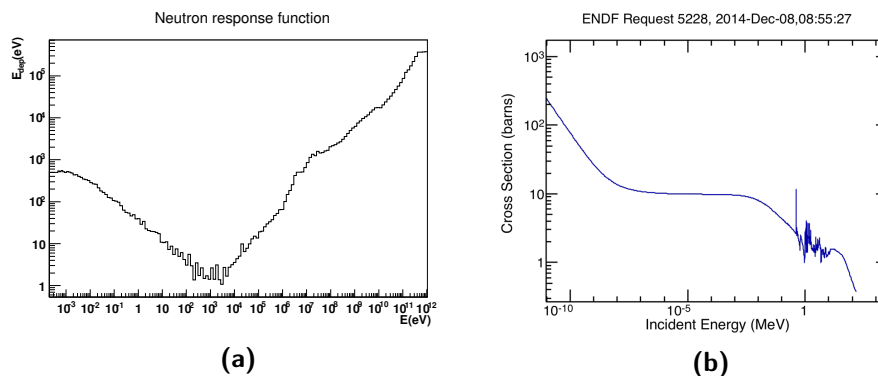


Figure C.2: In a) the nitrogen response function data from CERN is seen. In b), neutron cross section from ENDF is presented [32].

A histogram for gammas, corresponding to the one for neutrons, is shown in Figure C.3. This figure is of lower resolution and is presented in 90 bins. Below $5 \cdot 10^4 eV$, the graph shows zero energy deposition in the nitrogen. This is not a physical property rather than a limitation of the instrument. In other words, we can conclude that we do not have any information about energy deposition for incident gammas with energy below $5 \cdot 10^4 eV$. Furthermore, the measurements are saturated for gammas with energy above $2 \cdot 10^{11} eV$. This can be derived from simulation. It means that gammas with too high energy will not be absorbed in the given volume of the ionization chamber with nitrogen. The gamma deposits energy during its flight through the chamber but survives the entire flight and exits the chamber. Therefore, any gamma with too high energy will only show a deposition of about $10^6 eV$.

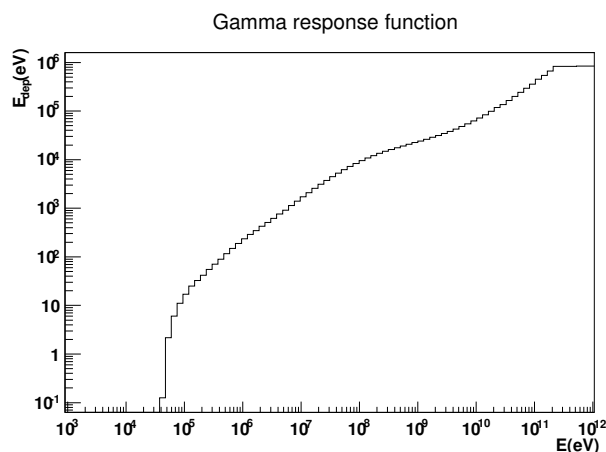


Figure C.3: The figure presents data from CERN, illustrating the nitrogen response function for gammas.

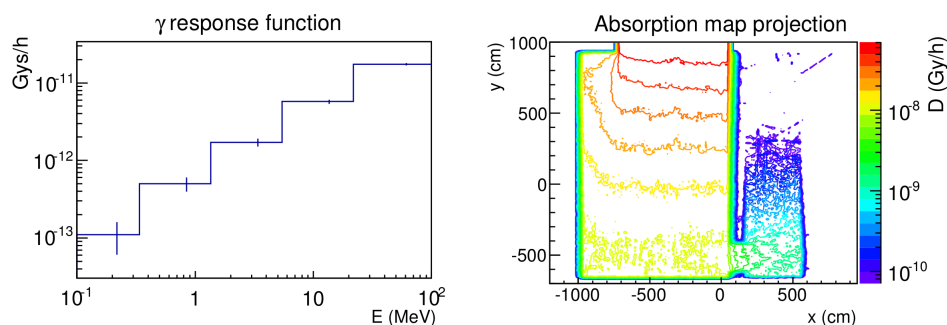


Figure C.4: Recomputed response function and absorption map.

The ionization chamber used in the simulation is a 8.9 cm cylinder with parallel plate electrodes separated by 0.5 cm in the simulation. There are 61 electrodes, or equivalently 60 active volumes and, hence, the total active volume of the chamber is:

$$V = n\pi\left(\frac{d}{2}\right)^2l$$

where n is the number of active volumes, d is the diameter and l is the distance between the plate electrodes, yielding a volume of $V \approx 0.75m^3$. The density of the nitrogen is $1.2kg/m^3$, i.e. there is approximately 0.90 kg nitrogen inside the chamber. With this, the response function can be converted into presenting Gy/γ by multiplying the detected charges with the ionization energy threshold to get the deposited energy in eV, convert the energy from eV to J and divide by mass. Preferably, the response function shall present Gys/h in order for the absorption map to display Gy/h. This can be derived from the flux in the radiation map, which is given in $\gamma cm^{-2}s^{-1}$ and there is 3600 seconds per hour. For gammas, the resulting response function and the absorption map can be seen in Figure C.4. Notice that the absorption map presents Gy/h on the z-axis.

Radiation Effects on Cameras

During a visit at Lund University Hospital, various devices were examined, e.g. radiation therapy equipment, CT scans and surveillance cameras in radiatory environments.

Interesting radiation effects were clearly manifested in the cameras. Evidently, a number of pixels were dead, which can be seen in Figure D.1. The bright spots are dead pixels, which was easily established when the camera was moving. The doctors of the hospital explained that the correlation between machine use that causes radiation, and dead pixels in cameras, is very clear.

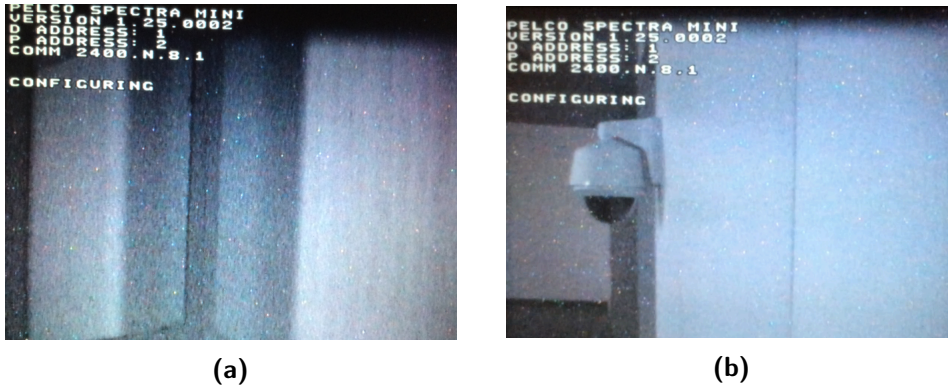


Figure D.1: In a) and b), camera images are shown. The bright dots seen in the figures, are dead pixels that are caused by radiation damages. The cameras are located in a room with a linear accelerator used for radiotherapy at Lund University Hospital.

L.E.N.A Experiment Guideline Proposal

On Wednesday December 10, a conference was held at ESS, Lund, in the matter of a collaboration with the SPES project (Selective Production of Exotic Species) at Istituto Nazionale di Fisica Nucleare (INFN). The collaboration regards research and experiments of radiation effects on materials and electronics at the L.E.N.A laboratory, Pavia University, Italy. The proposal of collaboration was presented by Alberto Andrichetto, LNL-INFN, and Aldo Zenoni, Brescia University and INFN Sezione di Pavia, Pavia University.

The conclusion and prospects of the aforementioned presentation was stated as the following:

- “
1. We are convinced that the RDS_SPES Project on radiation damage may be a timely and useful initiative for many European (and worldwide) facilities presently in construction in the field of nuclear physics and applications
 2. The atouts of the Project are the availability of the LENA Laboratory for irradiations and Materials Science Laboratories to perform pre and post irradiation tests on materials and components
 3. Possible collaborations and sharing of experience, knowhow and resources could be strategic to aim the project effort at best
 4. We hope that ESS could be the first outstanding new Partner of our Project”

It is hereby proposed that staff of the ESS defines an agreement of what electronics is preferable to undergo experiments in terms of irradiation and design of response function. Such response function should cover a relevant energy spectrum for each device, if possible. In other words, a device, which is only used in the FEB, may only need a response function in the interval (100 keV, 100 MeV) whilst the energy in the monolith may be up to an order of GeV. Furthermore, the response function should be of sufficiently high resolution, meaning that it should be able to represent energy intervals in a rebinned response function, such that all interesting energies are captured and with the same number of bins as the number of energies for which Monte Carlo simulations are made. It must be kept in mind, though, that it may be desired to have as high resolution as possible of the response function as the data may be used in a different application, either later at the ESS or at other research facilities.

All necessary information about the experiment setup must be thoroughly documented in order to enable the possibility of recalculating the results to generate

response functions that, upon folding with radiation maps, reveal the absorption in the desired unit, e.g. Gy/h.

After extensive experiments, it is recommended that the possibility for constructing a radiation weighting factor for electronics, similar to the one for human tissue, is considered.

The experiment guidelines presented in this appendix is substantiated by this thesis.



LUND
UNIVERSITY

Series of Master's theses
Department of Electrical and Information Technology
LU/LTH-EIT 2015-427

<http://www.eit.lth.se>